A MODEL OF THE CRUST AND UPPER MANTLE STRUCTURE OF THE HELLENIC AND CYPRUS SUBDUCTION ZONES CONSTRAINED BY GRAVITY AND SEISMIC DATA

by

SÜLEYMAN ALEMDAR

REZENE MAHATSENTE, COMMITTEE CHAIR
ANDREW M. GOODLIFFE
IBRAHIM ÇEMEN
TONY SMITHSON

A THESIS

Submitted in partial fulfillment of the requirements
for the degree of Master of Science
in the Department of Geological Sciences
in the Graduate School of
The University of Alabama

TUSCALOOSA, ALABAMA

2015

ABSTRACT

The Aegean-Anatolian region is one of the most dynamically complex and seismically active tectonic settings on Earth. The dynamic evolution of this region is dominated by the African plate subduction along the Hellenic and Cyprus trenches and collision between the Anatolian and Eurasian plates. The region is characterized by active volcanism, large-scale continental extension, uplift, slab rollback, slab break-off and slab-tear.

Several seismic tomography studies suggest the presence of a low-velocity zone in the upper mantle beneath southwestern Anatolia. The low-velocity zone is interpreted as asthenospheric material rising up through a slab window (slab-tear) in the subducting African plate. The slab-tear and possible detachment of the subducting African lithosphere from the surface plates are attributed to the differential retreat rates between the Hellenic and Cyprus trenches. The hot asthenosphere might have induced thermal erosion on the crust beneath southwestern Anatolia.

To determine the effects of the hot asthenospheric material on crustal structure, 2.5-D and 3-D gravity models of the Aegean-Anatolian region (24°-33° E and 34°-40° N) have been developed. The gravity model is based on satellite-derived and terrestrial gravity data from the European Improved Gravity Model of the Earth (EIGEN-6C2). The EIGEN-6C2 model includes terrestrial and satellite gravity data from GRACE (Gravity Recovery and Climate Experiment) LAGEOS (Laser Geodynamics Satellites), and GOCE (Gravity field and steady-state Ocean

Circulation Explorer) missions. The results of the gravity modeling, as constrained by geophysical data and models such as receiver function and seismic tomography, show that the crust above the low-velocity zone is relatively thin. The crustal thickness within the asthenospheric window area ranges from 24 to 29 km, and the thickness increases outside the asthenospheric window area (30 - 42 km). The observed crustal thinning might be attributed to thermal erosion induced by upwelling hot asthenosphere and extensional tectonics related to the Southwest retreating Hellenic trench and westward movement of the Anatolian micro plate. The magmatic centers and high geothermal gradients in the Menderes Massif Complex are indicative of an upwelling asthenosphere beneath southwestern Anatolia. Thus, asthenospheric flow may have played a role in the genesis of the crustal structure of southwestern Anatolia.

DEDICATION

Most people say that it is the intellect which makes a great scientist. They are wrong: it is character.

– Albert Einstein

I dedicate this thesis to my family and extended family. A special feeling of gratitude goes to my parents, Mustafa and Müzeyyen, who have always encouraged me.

I also dedicate this thesis to my brother Lokman and his wife Ayşe. In addition; I dedicate this work and give special thanks to my brother Hasan, who have been not only my brother but also a good friend, and his wife Kübra.

This thesis is dedicated to my sisters Ayşe and Zeynep who have been helping me a lot throughout my whole life. This work is dedicated to Hülya and Ilhami Boztepe who have been showing their hospitality and generosity to me.

Last but not least, I want to dedicate this work to my relatives.

LIST OF ABBREVIATIONS AND SYMBOLS

2.5-D Two and a half dimensional

3-D Three dimensional

AB Antalya Basin

AM Anaximander Mountains

ATB Anatolide-Tauride Block

BA Bouguer anomaly

BSZ Bitlis-Zagros Suture

Ca. Approximately

CAP Central Anatolian Province

EACP East Anatolian Contractional Province

EAFZ East Anatolian Fault Zone

EGM Earth Gravitational Model

EIGEN European Improved Gravity model of the Earth

ESM Eratosthenes Sea Mount

f Fourier transform

g Gravitational acceleration

G Gravitational constant

HB Herodotus Basin

HSZ Hellenic Subduction Zone

IAESZ İzmir-Ankara-Erzincan suture zone

IGF80 International Gravity Formula 1980

IZ Istanbul Zone

K Bulk modulus

KAIVF Kirka-Afyon-Isparta Volcanic Field

Km Kilometer

KVF Kula Volcanic Field

LB Levantine Basin

m/s Meters per second

m Meter

Ma Millions of years before present

mGal Unit of gravitational acceleration

mW/m^2 MilliWatt per square meter

μ Shear modulus

NAFZ North Anatolian Fault Zone

ρ Density

s Second

SZ Sakarya Zone

WAEP Western Anatolian Extensional Province

WGS84 World Geodetic System 1984

γ_n Normal gravity field

λ_c Cut-off wavelength

ACKNOWLEDGEMENTS

I could not have accomplished this research without the support and counseling of my thesis committee, colleagues, friends, and family.

I am deeply indebted to my advisor Dr. Rezene Mahatsente for his patience, encouragement, guidance, invaluable comments, suggestions, provisions and friendship; I appreciate the effort he made to share his geophysical research expertise with me. It would not have been possible to complete this thesis without his exceptional support at any step of the research. I will always gratefully acknowledge his constant generous guidance throughout my academic past.

I would also like to express my sincere gratitude to Dr. Ibrahim Çemen for his invaluable assistance and support at various stages of the thesis study.

I owe a deep sense of gratitude to Dr. Andrew Goodliffe for his precious input, inspiring advices and support for this thesis.

I am extremely thankful and grateful to Mr. Tony Smithson for his endless support, help and sharing his knowledge of geophysics that helped me throughout my academic life.

I would like to acknowledge and thank the generous help by Jim Donahoe, Debbie Frank, Karen Linville, and Beth Partlow.

Dr. Fred Andrus is acknowledged not only for helping me but also for being a nice, great and kind department chair.

Sincere thanks to my graduate lab mate Jeff Clark and the faculty and staff of the Department of Geological Sciences, The University of Alabama.

I would like to extend a special thanks and recognition to my parents for their guidance, wisdom, encouragement, and patience over the years. Their belief in me has always helped me to survive the stress throughout my life.

Sincere thanks to my friend and colleague Burak Tüfekçioğlu who has been a good friend and supporter throughout my academic life.

I am also pleased to have this opportunity to thank Kocaeli University faculty members Prof. Dr. Mithat Fırat Ozer, Prof. Dr. Şerif Barış, and Asst. Prof. Ertan Pekşen who encouraged me to have this opportunity.

It is my privilege to thank Mr. Ahmet Selvitop and Mesut Hazar for their constant encouragement and help throughout the stressful admission process and my thesis research period.

Finally, I would like to thank Turkish Petroleum Company for providing this academic education opportunity, scholarship and data. I am grateful to my technical as well as educational advisers from Turkish Petroleum Company.

CONTENTS

LIST OF TABLES

LIST OF FIGURES

1. INTRODUCTION

The Aegean-Anatolian region is one of the most dynamically complex tectonic settings on Earth (Figure 1). The tectonics of the region is mainly driven by African plate subduction along the Hellenic and Cyprus trenches, northward collision between the Arabian and Eurasian plates and the North and East Anatolian Fault Zones (NAFZ and EAFZ, respectively).

The region is one of the best developed examples of continental extensional tectonics (Hetzel and Reischmann, 1996; Gautier et al., 1999; Lips et al., 2001; Catlos and Çemen, 2005; Çemen et al., 2006) and is characterized by active seismicity, volcanism, uplift, slab-rollback and slab-tear (Christova et al., 1993; Akyol et al., 2006; Zhu et al., 2006; Sayil & Osmanşahin 2008; Aydan & Kumsar 2014; Çemen et al., 2014). The origin and mechanism of extensional tectonics in the region still remains controversial.

The Hellenic and Cyprus subduction zones and southwestern Anatolia are the key elements in the active tectonics of the Eastern Mediterranean. There are regional velocity models for the Aegean based on body wave (Romanowicz, 1980; Spakman et al., 1993; Al-Lazki et al., 2004) and surface wave velocities (Levshin et al., 1992, 1994; Marquering & Snieder 1996; Ritzwoller & Levshin 1998; Villasenor et al. 2001; Marone et al., 2003; Pasyanos 2005; Kustowski et al., 2008).

The crust and upper mantle structure of Turkey has also been studied as a part of several seismic projects in the Mediterranean (Panza et al., 1980; Spakman et al., 1991, 1993; Koulakov et al., 2002; Piromallo & Morelli 1997, 2003; Meier et al., 2004; Erduran et al., 2008). The

detailed upper mantle structures beneath southwestern Anatolia are known from studies of body and surface wave tomography (Mindevalli and Mitchell, 1989; Tezel et al., 2007; Di Luccio et al., 2007; Erduran et al., 2009; Cambaz & Karabulut, 2010; Biryol et al., 2011; Bakırcı et al., 2012; Salaün et al., 2012; Sayil et al., 2014; Delph et al., 2015; Kind et al., 2015). Seismic tomography studies suggest the presence of low- velocity material in the upper mantle beneath southwestern Anatolia between the Hellenic and Cyprus trenches (Figure 2; Biryol et al., 2011; Salaün et al., 2012). The low-velocity zone is interpreted as a slab-tear (asthenospheric window) in the subducting African plate (Spakman et al., 1993; Piromallo and Morelli 2003; Chang et al., 2010; Biryol et al., 2011; Salaün et al., 2012). The slab-tear is attributed to the differential retreat rates between the Hellenic and Cyprus trenches (Altunkaynak and Dilek 2006; Jolivet et al., 2013; Gessner et al., 2013; Çemen et al., 2014).

The hot asthenospheric material may have caused thermal erosion and modified the overlaying crystalline basement and uppermost mantle structure beneath southwestern Anatolia. The observed crustal thinning in southwestern Anatolia may partly be caused by thermal erosion and extensional tectonics. Although a variety of geophysical and geological studies have been performed in adjacent areas of southwestern Anatolia, the detailed structure of the slab-tear (asthenospheric window) and its effect on the overlaying crust is still largely unknown.

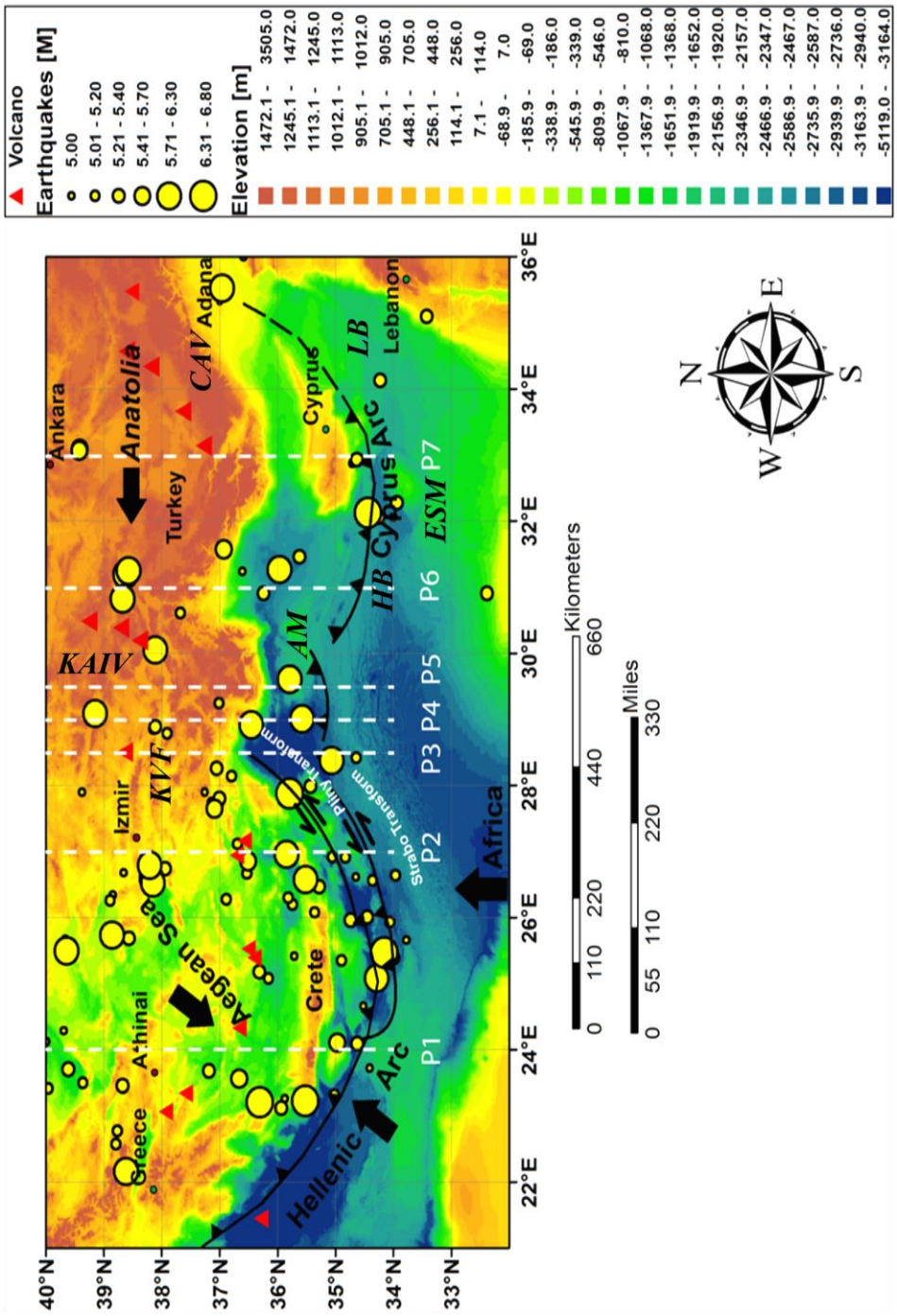

Figure 1. Topographic map of the Aegean-Anatolian region. The white dashed lines show the locations of the 2.5-D gravity models. Black arrows indicate the directions of plate motions. Red triangles are for volcanoes. The yellow circles indicate earthquake hypocenters (events from 1985 to 2015: http://udim.koeri.boun.edu.tr/zeqdb/indexeng.asp). Bathymetric data are from ETOPO-1 global relief model (Amante & Eakins, 2009). Abbreviations: KVF, Kula Volcanic Field; KAIVF, Kirka-Afyon-Isparta Volcanic Field; AM, Anaximander Mountains; ESM, Eratosthenes Sea Mount; HB, Herodotus Basin and; LB, Levantine Basin.

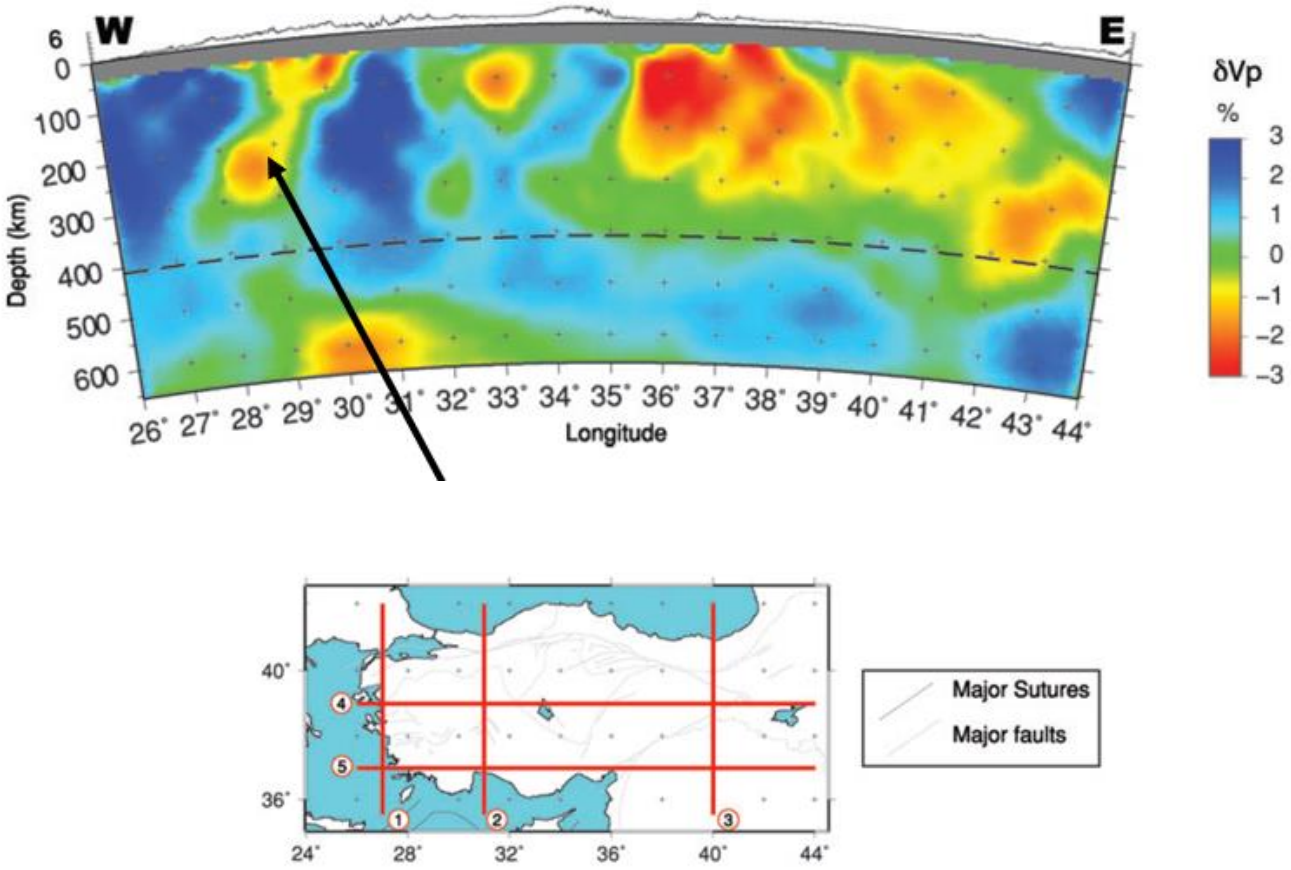

Figure 2. (Top) Seismic tomography of the eastern Mediterranean (Biryol et al., 2011). The low-velocity zones are shown in yellow and red. The black arrow indicates upwelling hot asthenospheric material beneath southwestern Anatolia. **(Bottom)** Locations of the seismic tomography profiles.

In this study, the effect of the hot upwelling asthenospheric material on crustal structure in southwestern Anatolia has been assessed using satellite and terrestrial gravity data modelling. The gravity data is based on the European Improved Gravity Model of the Earth (EIGEN-6C2; Förste et al., 2012). The density model is constrained by all available geophysical (receiver function, seismic tomography) and geological information and reveals the detailed structure of the crust and the low-velocity zone in the upper mantle.

2. GEOLOGICAL AND TECTONIC SETTING

The Aegean region is bounded to the north by stable continental Eurasia, to the south by the subducting African plate along Hellenic subduction zone (HSZ), to the east by the Anatolian plate and Cyprus Arc, and to the west by the Hellenides. The Aegean-Anatolian region is one of the most seismically active and rapidly deforming parts of the Alpine-Himalayan mountain belt formed by the convergence of the Eurasian, African and Arabian Plates. The convergence that came after the Cenozoic closure of the Tethys Ocean between the Eurasian and the northward-moving African Plates is considered to be the main driving processes of the present tectonics in the Aegean-Anatolian region (Şengör and Kidd, 1979; Dewey and Şengör, 1979; Taymaz et al., 1990; Jackson et al., 1992; Armijo et al., 1999; Taymaz et al., 2004; Faccenna et al., 2014; Schildgen et al., 2014) (Figure 3). The present-day kinematics of the Aegean is characterized by a counterclockwise rotation of the Aegean and Anatolian plates and internal extension of these plates (McKenzie, 1972, 1978; Le Pichon et al., 1995; Cocard et al., 1999; Kahle et al., 1999; McClusky et al., 2000).

The Anatolian plate can be divided into three main provinces (Şengör et al., 1985): East Anatolian Contractional Province (EACP), where compressional tectonism is driven by collision between Eurasian and Arabian Plates along the Bitlis-Zagros Suture (BZS); Western Anatolian Extensional Province (WAEP), where extension is dominant due to westward motion of the

Anatolian plate and slab roll back along the Aegean trench; and the Central Anatolian Province (CAP) (Figure 3). The region includes six major lithospheric blocks namely the Strandja, the Istanbul, the Sakarya, the Anatolide -Tauride Block, the Kirsehir Massif and the Arabian Platform (Şengör and Yilmaz, 1981; Şengör et al., 1982; Okay, 1989; Okay et al., 1994; Figure 4). The study area (Figure 3) covers the Western Anatolia Extensional Province (WAEP) and the western half part of the Central Anatolia Province (CAP). This includes the Istanbul and Sakarya zones, the Kirsehir Massif, and the Anatolide-Tauride block (Figure 4).

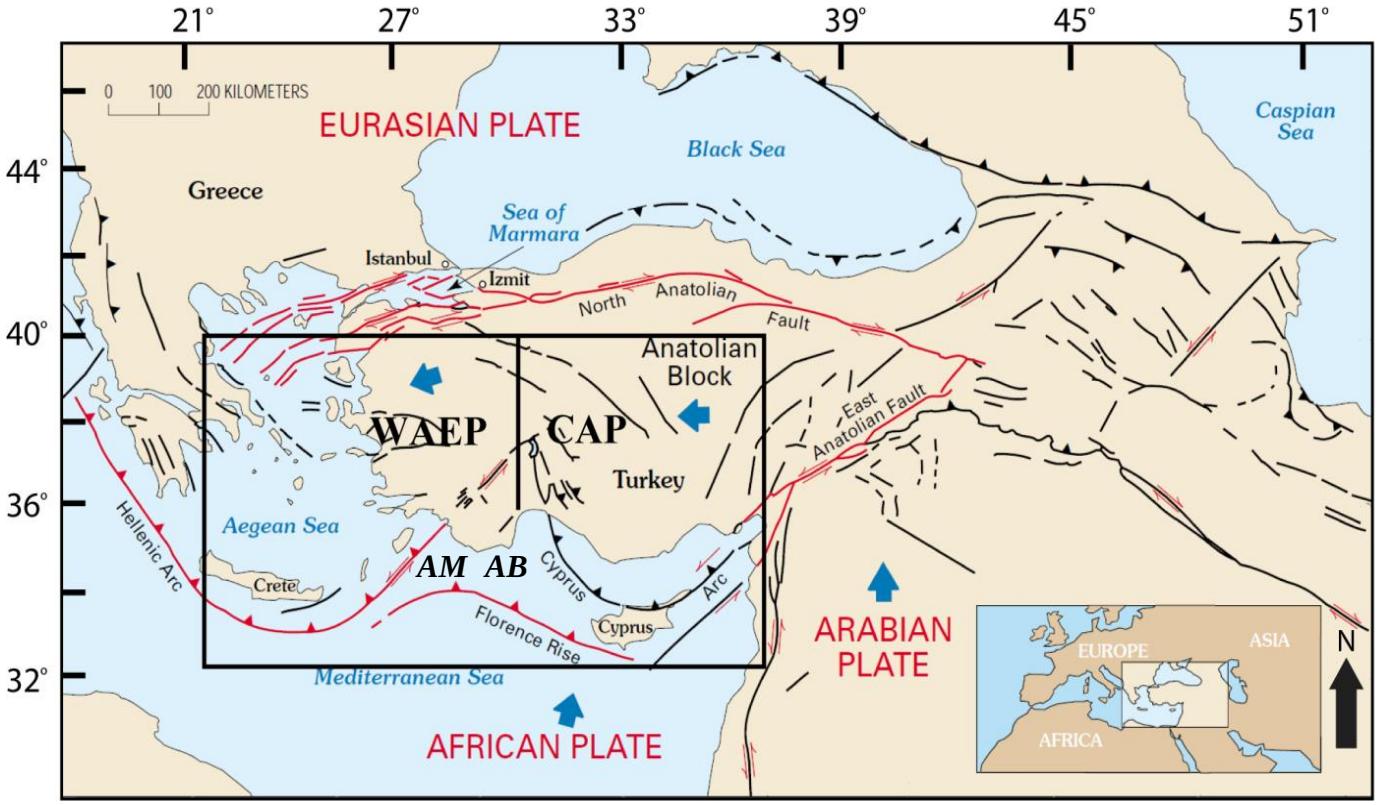

Figure 3: Tectonic map of Turkey and the Aegean region. Major tectonic features are the North Anatolian fault, East Anatolian fault and the Hellenic and Cyprus trenches (Modified after Barka et al., 1992; Rockwell et al., 2001). The black rectangle shows the study area for the 2.5-D and 3-D gravity modeling (24°E-33° E and 34°N-40° N). Abbreviations: WAEP and CAP stand for Western Anatolia Extensional Province; and Central Anatolia Province, respectively. AM, Anaximander Mountains and, AB, Antalya Basin.

The Istanbul Zone (IZ) consists of a well-developed Ordovician to Carboniferous age sedimentary sequence. The IZ covers the top of a late Precambrian crystalline basement (Okay et al., 1999; Chen et al., 2002; Yiğitbaş et al., 2004; Ustaömer et al., 2005) and is bounded by the Intra-Pontide suture in the northern part of study area (Şengör & Yılmaz 1981). The Sakarya Zone (SZ) is bounded by İzmir-Ankara-Erzincan suture zone (IAESZ). The complex basement consists of metamorphic sequence of gneiss and Paleozoic granitoids (Delaloye and Bingöl 2000; Okay et al., 2002; 2006; Topuz et al., 2007) and underlies sedimentary sequence of lower Jurassic sandstones (Okay et al., 1999).

The Kirsehir Block is consisting of late Cretaceous felsic intrusives and metamorphic rocks and is folded and multiplies deformed (Akiman et al., 1993; Okay and Tuysuz 1999; Whitney & Hamilton 2004). The Anatolide-Tauride Block (ATB) consists of marine sedimentary sequences on the surface resulting from the closure of the Neotethys Ocean in the Late Cretaceous (Okay and Tuysuz 1999). The ATB is bounded by the Inner-Tauride Suture zone and shares the same Paleozoic stratigraphy with the Arabian platform (Okay et al., 1999; Monod et al., 2003).

2.1 The Western Anatolia Extended Terrane

Western Anatolia, which is characterized by metamorphic complexes, has been undergoing N-S extension since Late Oligocene-Early Miocene due to the tectonic movements of the Anatolian plate. Western Anatolia is dominated by extensional deformation associated with the slab rollback of the subducting African lithosphere. The initiation and cause of the extension remains controversial. Cenozoic extensional tectonics in western Anatolia was initiated in the

Late Oligocene-Early Miocene in the Rhodope region (Seyitoğlu et al., 1992; Yilmaz et al., 2000; Lips et al., 2001; Catlos and Çemen; 2005; Çemen et al., 2006; Jolivet and Brun, 2010).

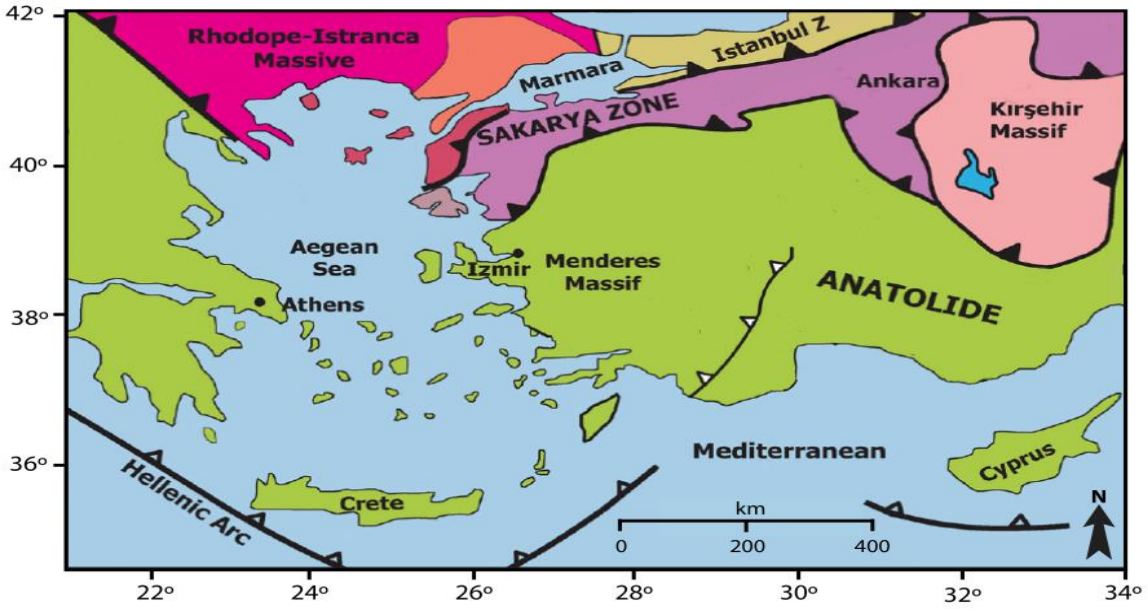

Figure 4: Major tectonic features and blocks in the Aegean and Anatolia: The Hellenic and Cyprus arcs, Anatolide-Tauride block, Kirsehir Massif, Sakarya zone, Istanbul zone and the Rhodope-Istranca Massif (modified after Yolsal-Cevikbilen et al., 2012).

The proposed mechanisms of Cenozoic extension can be grouped as; a) post-collisional extension generated in response to crustal thickening after the collision between the Tauride – Anatolide Platform and the Sakarya Continent (Seyitoğlu et al., 1992); b) westward escape or lateral extrusion of the Anatolian plate along the North and East Anatolian Fault Zones (Şengör and Yılmaz, 1981; Şengör et al., 1985; Çemen et al., 1999) due to collision of the Eurasian and Arabian plates along the Bitlis-Zagros suture zone (BZS); c) subduction roll-back and associated back-arc extension (Le Pichon and Angelier, 1981; Meulenkamp et al., 1988, 1994; Spakman et al., 1988; Jolivet and Brun, 2010; Jolivet et al., 2013); and d) a three-stage continuous simple

shear extensional model as a result of the mechanisms listed above (Çemen et al., 2006; Gessner et al., 2013).

2.2 The Cyprus Trench

The Cyprus Arc is part of the convergent margin between the African and the Aegean-Anatolian plates. The northwestern side of Cyprus is bounded by the Anaximander Sea Mountains, the Florence Rise and the Antalya basin (Figure 3). Subduction is active beneath the whole length of the Hellenic trench, whereas the Cyprian arc is undergoing subduction along its northwestern margin (Wdowinski et al., 2006). Strike-slip faults cause westward movement of Cyprus, similar to the westward escape of the Anatolian plate (Harrison et al., 2004; Elitok and Dolmaz, 2008). The western side of Cyprus experiences extensional tectonics (Pınar and Kalafat 1999). The Pliny Transform Fault (Figure 1) is accommodating the differential motion between the Hellenic and Cyprus trenches (McClusky et al., 2003; Schattner et al., 2010).

Cyprus is divided into four geological zones: (a) the Pentadaktylos (Kyrenia) Zone consists of massive rocks of Permian–Carboniferous to Lower Cretaceous age basement; (b) the Troodos Zone or Troodos Ophiolite formed during oceanic spreading and the formation of oceanic crust in the Upper Cretaceous; (c) the Mamonia Zone or Complex consists of a series of igneous, sedimentary and metamorphic rocks, ranging in age from Middle Triassic to Upper Cretaceous (230–75 Ma); and, (d) the autochthonous sedimentary rocks ranging in age from Upper Cretaceous through to Pleistocene (67 Ma to recent) and cover the area between the Pentadaktylos and Troodos Zones.

2.3 The Hellenic Trench

The Hellenic subduction zone (HSZ) is part of the active convergent margin between the African and Eurasian plates in the Mediterranean region. The subduction zone plays a key role in the active tectonics of the eastern Mediterranean as well as in the Nubia-Arabia-Eurasia plate interaction (McKenzie et al., 1972; Le Pichon and Angelier, 1981; Jolivet and Faccenna, 2000). It is dominated by the north-northeasterly subduction of the African plate beneath the Aegean plate. The island of Crete occupies a prominent position in the fore-arc of the subduction near the strongly curved plate boundary. The volcanic arc north of Crete is bounded by the Cycladic islands including the active volcanic centers of Santorini and Milos. The western Hellenides are deforming by thrust, normal and wrench faulting and westwards movement of the Hellenic napes due to crustal shortening. This is expressed by high seismicity and intense tectonic deformations of the upper crust and sediments (Makris 1978; McKenzie 1978; LePichon & Angelier 1979; Papoulia & Makris 2010). The HSZ shows a Wadati –Benioff zone dipping at ∼30° and ∼45° and extending from 20 - 100 km and 100 - 150 km depths, respectively (Papazachos et al., 2000). The rate of convergence of the Hellenic system is ∼40 mm/yr. (McClusky et al., 2000).

3. PREVIOUS GEOPHYSICAL STUDIES

The Aegean-Anatolian region has been the subject of research for several years. The results of these studies have been used to constrain the gravity model for this study. In the subsequent sections, the previous geophysical studies in Anatolia, Crete and Cyprus are described.

3.1 Gravity

3.1.1 Anatolia

The crustal structure of Turkey was investigated by several researchers using gravity data modeling. The crustal thickness in Turkey, as determined from gravity data modeling, ranges from 28 km in southwestern Anatolia to 50 km in eastern Turkey (Tirel et al., 2004; Bilim et al., 2007; Ates et al., 2012; Makris et al., 2013).

Sediment thickness in the Büyük Menderes and Gediz grabens varies significantly. The average depth to basement in the Büyük Menderes and Gediz grabens varies from 1.5 to 3.5 km, with the shallowest depth being in the Gediz graben (Paton, 1992; Gürer et al., 2002; Sari et al., 2006; Işık et al., 2009).

3.1.2 Aegean

The Moho depth map of the Aegean region, as derived from gravity data modeling, shows varied crustal thicknesses. The average crustal thickness in western Greece, the Aegean Sea and the Hellenides are 32 km, 20 - 25 km, and 40 - 49 km, respectively (Le Pichon and Angelier, 1979; Makris and Stobbe, 1984; Tsokas and Hansen, 1997; Tiberi et al., 2001; Tirel et al., 2004; Casten et al., 2006). The crustal thickness in the Aegean, as inferred from marine gravity data inversion, increases from ~ 22 km in the Cretan Sea to ~ 25 km in Cyclades (Tirel et al., 2004).

3-D gravity models of the Hellenic subduction zone and the western Hellenides show variable Moho depth and sediment thicknesses. The sediment thickness ranges from 8 km in western Hellenides to 18 km in western Crete and Mediterranean Ridge (Casten et al., 2006; Makris et al., 2013).

3.1.3 Cyprus

There are few gravity studies of the crust, upper mantle and sedimentary structures of the Cyprus arc. The crustal thickness in Cyprus, as determined from gravity data inversion, ranges from 28 to 30 km (Salah et al., 2014). The average sediment thickness in Cyprus based on gravity data modeling is ~10 km (Ergün et al., 2005).

3.2 Seismic

3.2.1 Anatolia

Various geophysical studies have been conducted to determine the shear wave velocity structure of the upper mantle and crust in southwestern Anatolia. This includes receiver function analysis (Saunders et al., 1998; Çakır et al., 2000; Zor et al., 2003; Çakır and Erduran, 2004; Angus et al., 2006; Zhu et al., 2006; Zor et al., 2006; Özacar et al., 2008; Erduran, 2009; Tezel et al., 2010,2013; Çakır and Erduran, 2011; Vanacore et al., 2013; Karabulut et al., 2013; Sodoudi et al., 2015; Delph et al., 2015) and seismic wave tomography (Necioğlu et al., 1981; Van Der Meijde et al., 2003; Biryol et al., 2011; Salaün et al., 2012; Fichtner et al., 2013; Delph et al., 2015). The results of these studies show that crustal thickness increases from 23 km in the Aegean to 50 km in Anatolia. Regional variations in crustal thickness were also inferred from estimates of surface wave group velocities and Pn tomography (Tezel et al., 2007; Cambaz and Karabulut, 2010; Landès et al., 2010; Mutlu and Karabulut, 2011).

Crustal thickness in the western and central Anatolia ranges from 25 to 47 km, and the crust is thin compared to eastern Anatolia (Saunders et al., 1998; Horasan et al., 2002; Karagianni et al., 2005; Akyol et al., 2006; Zhu et al., 2006; Zor et al., 2006; Di Luccio and Pasyanos 2007; Tezel et al., 2007, 2010, 2013). The minimum crustal thickness (25 km) was observed beneath the Menderes Massif (Karabulut et al., 2013). The thinning is mainly attributed to the extensional tectonics in the Aegean region (McKenzie et al., 1978; Le Pichon and Angelier 1979; Jackson et al., 1994; Reilinger et al., 1997; McClusky et al., 2000; Reilinger et al., 2006; Sayil et al., 2014).

The thickness of the upper-crust in southwestern Anatolia varies from 14 km to 16 km (Akyol et al., 2006; Zhu et al., 2006; Di Luccio et al., 2007; Tezel et al., 2007,2010, 2013; Sayil et al., 2014; Salah et al., 2014).

Seismic tomography studies in southwestern Anatolia reveal a major slab-tear in the subducting African plate between the Hellenic and Cyprus trenches (Amaru, 2007; van Hinsbergen et al., 2010; Mutlu and Karabulut, 2011; Biryol et al., 2011; Bakırcı et al., 2012; Salaün et al., 2012). The asthenospheric window between the Hellenic and Cyprus slabs could not be seen by Kind et al., (2015) due to lack of resolution. High (p-wave velocity/s-wave velocity) Vp /Vs ratio have also been obtained in western and central Anatolia. This possibly indicates the existence of partial melt in the lower crust and uppermost mantle (Horasan et al., 2002; Zor et al., 2003; Erduran et al., 2007; Ersan and Erduran 2010; Özacar et al., 2010; Bilim et al., 2011; Çakır and Erduran 2011; Vanacore et al., 2013; Tezel et al., 2013; Salah et al., 2014).

3.2.2 Aegean

Several seismic studies have been conducted in the Aegean to image the structure of the Hellenic subduction zone (Spakman et al., 1988, 1993; Papazachos and Nolet, 1997; Bijwaard et al., 1998; Papazachos et al., 2000; Piromallo and Morelli, 2003; Schmid et al., 2004; Suckale et al., 2009; Chang et al., 2010; Biryol et al., 2011; Gesret et al., 2011; Salaün et al., 2012; Pearce et al., 2012). The African slab penetrates down to the lower mantle with an average dip of about 40°-50° (Ligdas et al., 1990; Wortel and Spakman, 2000; Faccenna et al., 2006; Biryol et al., 2011; Salaün et al., 2012). The tip of the subducting African lithosphere in the Aegean has been

imaged down to a depth of about 225 km beneath the volcanic arc using converted S - P waves (e.g. Sodoudi et al., 2006).

High seismic activity occurs along the Hellenic arc (Papazachos and Comnikakis, 1971; Hatzfeld and Martin, 1992; Knapmeyer et al., 1999; Papazachos et al., 2000). Papazachos et al., (2000) identified a Wadati-Benioff zone at a depth of 180 km below the central Aegean from seismological observations. The zone starts at a depth of 20 km under the convex side of the sedimentary part of the arc and dips towards the back-arc area, with a dip angle ~30° for shallow depths (~ 100 km) and ~45° for greater depths (~ 200 km). The Wadati-Benioff zone steepens from west towards the eastern part of the Hellenic subduction zone.

3.2.3 Cyprus

Continuous subduction of the "Western Cyprus slab" down to at least 138 km depth between western Cyprus and the Hellenic arc is supported by recent analyses of seismic (Kalyoncuoğlu et al., 2011; Imprescia et al., 2012; Schildgen et al., 2012b) and earthquake data (Koulakov et al., 2002; Piromallo and Morelli; 2003; Netzeband et al., 2006; Biryol et al., 2011; Bakırcı et al., 2012). The fast velocity anomaly associated with the subducting Cyprus slab is located north of Cyprus using P-wave and surface wave tomography (Koulakov et al., 2002; Piromallo and Morelli, 2003; Biryol et al., 2011; Bakırcı et al., 2012).

The average crustal and sedimentary thicknesses in Cyprus range from 12 to 35 km and 10 to 14 km, respectively (Makris et al., 1983; Ginzburg et al., 1987; de Voogd et al., 1992; Ben-Avraham et al., 2002; Koulakov & Sobolev, 2006; Vanacore et al., 2013). The thinnest crust in Cyprus is beneath Levantine Basin.

3.3 Geothermal

3.3.1 Aegean & Anatolian

The Aegean-Anatolian region is characterized by high heat flow values (average 83.8 mW/m^2 ; Lee and Uyeda, 1965; Langseth and Taylor, 1967; McKenzie et al., 1967; Gorshkov et al., 1972; Zonenshain et al., 1975). The high heat flow in the Aegean Sea is associated with two extensional tectonic regions (Fytikas et al., 1980). The first region extends along Palegonian - Parnos zone (interior side of the Hellenic island arc) and passes through the Astipalia and Kavaros islands and reaches Bodrum – Karaada. The heat flow value in this region is higher than 120 mW/m^2. The second region is in the Central Aegean (near to the western end of Izmir – Ankara zone) where the heat flow values there exceed 100 mW/m^2. The average heat flow value in Izmir is 101 mW/m^2 and reaches a maximum of 229 mW/m^2 (Akin et al., 2014).

The heat flow data determined by Tezcan (1979) and Tezcan and Turgay (1989) indicate some regional heat flow anomalies (120 mW/m^2) in the western Anatolia extended terrane (WAET). The average heat flow values for Western Anatolia based on silica geothermometry and conventional heat flow measurement are 107±45 mW/m^2 and 97±27 mW/m^2, respectively (Ilkişik et al., 1995; Akin et al., 2014). Curie point depths in western Anatolia are very shallow (about 10 km). The sub-continental mantle temperatures exceed the normal temperature range, because of the wide-range of young basaltic volcanism of Plio-Quaternary age (Bilim et al., 2007; Çoban et al., 2007).

4. BASICS OF GRAVITATIONAL FIELD

4.1 Gravitational Force

Newton's law of universal gravitation is a mathematical description, which states that each particle of matter in the universe attracts all others with a force directly proportional to its mass and inversely proportional to the square of its distance of separation (Telford et al., 1990).

That is,

$$F = -G\frac{M_1 M_2}{R^2} \qquad 4.1$$

where, F is the force between two particles of masses M_1 and M_2.

R - distance between the two masses

G - gravitational constant ($6.670*10^{-11} Nm^2/kg^2$ in SI units).

The minus sign shows that g is attractive

4.2 Gravitational Potential & Gravitational Acceleration

The derivation of the gravitational field can be simplified by using the concept of potential. The potential U(r) at a point in a gravitational field is explained as the work needed for gravity to move a unit mass from an arbitrary reference point (mathematically infinity) to the that point in the survey. It is defined as:

$$U(r) = \int_{\infty}^{R} g.dr = -GM \int_{\infty}^{R} \frac{dr}{r^2} = \frac{GM}{R} \quad 4.2$$

The gravitational acceleration vector g(r) can be derived from the potential U(r) and is given as:

$$\nabla U(r) = \frac{F(r)}{m} = g(r) \quad 4.3$$

$$g(r) = \frac{\partial U}{\partial r} = G\frac{M}{r^2} \quad 4.4$$

where, G = gravitational constant, R = Distance from Center of M, U = Gravitational potential, F = Gravitational force

The unit of gravitational acceleration, g in gravity exploration is “Gal”, in honor of Galileo Galile.

1 Gal = $10\ ms^{-2}$
1 mGal = $10^{-5}\ ms^{-2}$

4.3 Gravity Reduction

The gravity method of exploration is based on measurement of variations of gravity caused by density contrasts in subsurface structures. However, the observed gravity value at each station is affected by other factors (e.g. elevation, tide, latitude etc.). Thus, the gravity value at each station must be corrected before the data can be interpreted. Literally, gravity data reduction involves a series of processing steps to remove the unwanted signals from the observed data. In the subsequent sections, the standard reductions applied to gravity data are described.

4.3.1 Temporal variation

These are time dependent changes in the observed gravity. Literally, these alterations cause variations in acceleration that would be observed even if gravimeter's position has not been changed. These are instrumental drift and tidal variations.

4.3.1.1 Drift correction

Instrumental drift is the result of a change in the elasticity of the mass-spring system of gravity meters over time. The drift for each gravimeter is different (Figure 5). The observed gravity values are corrected using readings at a fixed base station. To be able to apply this reduction, the base station should be defined and readings at the base station should be repeated several times during measurement or survey.

4.3.1.2 Tidal correction

Tidal effects (Figure 5) result from the gravitational attraction of the sun and the moon because of their positional rotation with respect to the earth. Tides can be categorized based on their occurrence rate; the first component peaks approximately twice a day, the second peaks approximately daily, and longer period components peak every 14 days and 6 months as a result of the moon and the sun, respectively (Nettleton, 1976). Daily tidal predictions (0.1 - 0.3 mGal) can be obtained from global theoretical tidal models. In a typical gravity survey, the tidal correction is applied by repeated measurement at base station, usually at an interval less than the period of Earth tides. Also, daily tidal corrections can be obtained from tidal models and applied to observed gravity data.

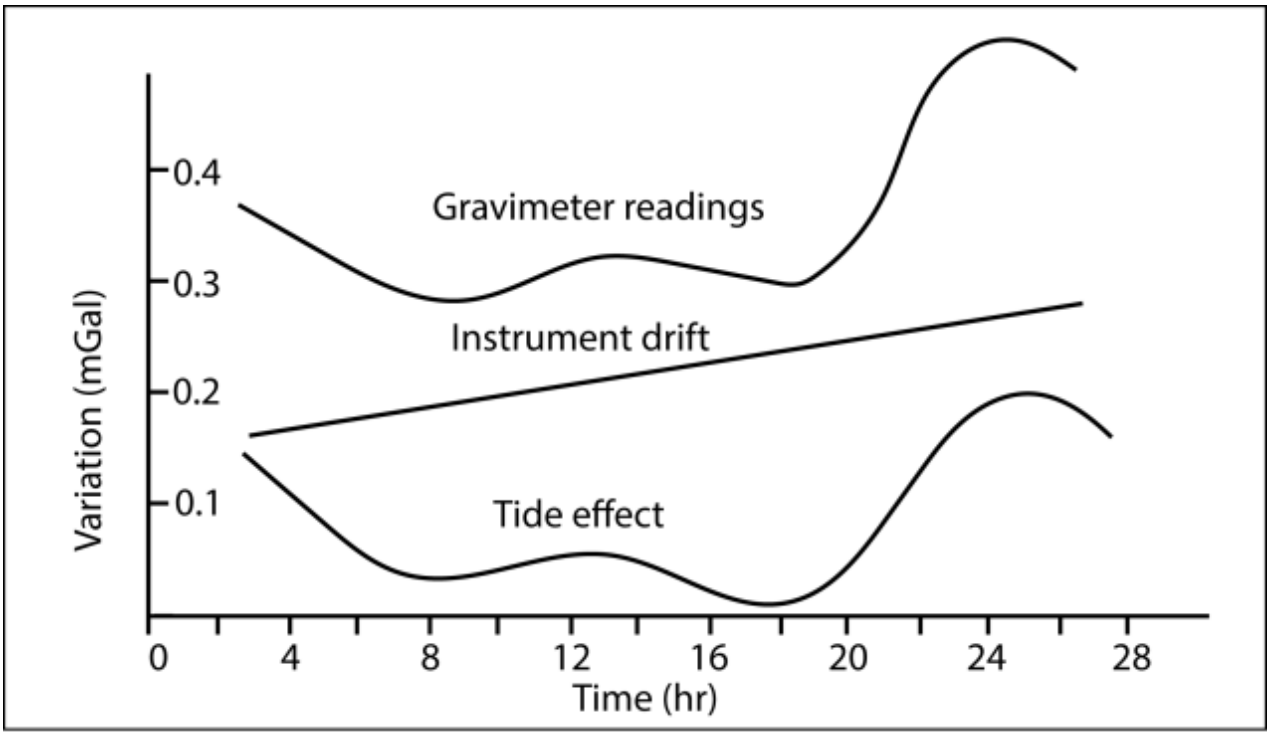

Figure 5. Typical gravimeter reading variation curve at a base station which is a combination of instrument drift and earth tidal variations (modified after Burger, 1992).

4.3.2 Spatial variation

Spatial variations are space dependent changes in the observed gravitational acceleration.

4.3.2.1 Latitude correction

The equatorial radius of the earth is greater than the polar radius. Thus, the gravity increases towards poles, and lower latitudes have higher gravity readings. The variation of gravity with latitude affects gravity reading and needs correction. Latitude correction takes into account the variation in gravity with latitude (from equator to pole). The correction is applied using the International Gravity formula (IGF80; Equation 4.5; Morelli et al., 1976)

$$\text{IGF80 (1980): } g_n = 978032.7\,(1 + 0.0053024\sin^2\varphi - 0.0000058\sin^2 2\varphi) \qquad 4.5$$

where ϕ is latitude

4.3.2.2 Free-air correction and Free air anomaly

The free-air correction takes into account variations in gravity with elevation (Figure 6). Hence, the free-air correction takes the difference in gravity between a datum (commonly the geoid or reference ellipsoid) and an observation point located above or below the datum where the gravity measurement is made.

The Free air correction term is given as:

$$\Delta G_{Free-air} = \text{-0.3086 [mGal/m]} \quad 4.6$$

The Free-air correction including the higher order terms in h is:

$$\Delta G_{Free-air} \approx$$

$$(0.30878 - 0.000439 \sin^2\varphi)h - (7.265 * 10^{-8} - 2.085 * 10^{-10} sin^2\varphi)h^2 \quad 4.7$$

where, *h* is the height of the gravity station in meters above a reference ellipsoid, φ is the latitude. Equation 4.7 includes the centrifugal acceleration. The free-air correction is added for a station above the datum, and subtracted for a station below the datum.

The free air anomaly is corrected for latitude and elevation variation and is defined as:

$$G_{\text{Free-air}} = g_{obs} - \gamma_n + 0.3086\ h \quad 4.8$$

Where γ_n - is the Normal gravity field of the Earth (value obtained after latitude correction), h is elevation and g_{obs} is observed gravity data.

4.3.2.3 Bouguer correction and the Bouguer anomaly

The Bouguer correction is used to account for a rock mass between a gravity station and a datum (Figure 7). The Bouguer correction consists of two main parts: 1) infinite Bouguer slab correction, which takes care of the attraction of the material between a station and a datum (correction is subtracted for a station above datum and added for a station below the datum), 2) Bullard correction (B), which takes care of the effects of Earth's curvature on the observed gravity data (black area in Figure 7).

The effect of nearby topography on gravity stations is reduced using terrain correction (T). The terrain correction (T) is applied to the Bouguer corrected gravity values. The correction is always added to a gravity station.

The Bouguer correction term is given as:

$$B_c = 2\pi G h \rho = 0.0419\, h\rho \quad (\text{mGal}) \qquad 4.9$$

Where ρ is the density (2.67 g/cm^3) and h is elevation above the datum in meters.

The Bouguer anomaly is given as:

$$g_{Bouguer} = g_{obs} - \gamma_n + 0.3086\, h - 0.0419\, h\rho - B + T \qquad 4.10$$

where ρ: density of the infinite slab (generally 2.67 g/cm^3), γ_n is the Normal gravity field of the Earth (value obtained after latitude correction) in mGal, B is Bullard correction and T is Terrain correction.

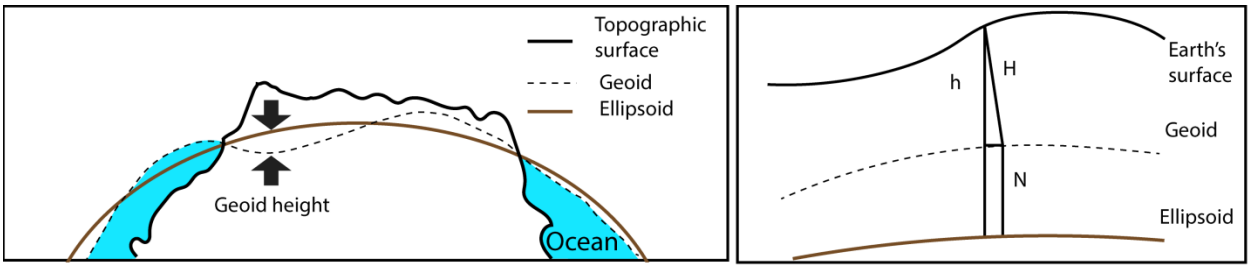

Figure 6. Height system. Abbreviations: h: ellipsoidal height, H: height above the geoid, N = geoid undulation.

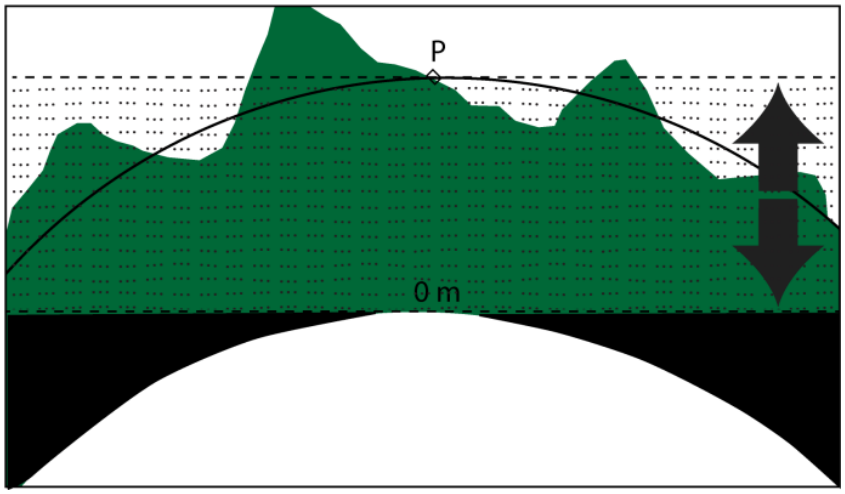

Figure 7. Bouguer slab correction.

4.3.3 Density determination

Gravity modeling requires that the densities of the subsurface structures are well defined. There are several ways to determine density: The Nettleton method (Nettleton ,1976), density logger, borehole gravity reading, density from free-air anomaly and empirical relation between seismic wave velocity and density. The density of subsurface structures is related to seismic wave velocities via elastic moduli. The relation between density and P & S-wave velocities is given as:

$$V_p = \frac{K+\frac{4}{3}\mu}{\rho} \quad 4.11$$

$$V_s = \sqrt{\frac{\mu}{\rho}} \quad 4.12$$

where V_p: Primary (compressional) wave, V_s: Secondary (shear) wave, ρ: Density, K: Bulk modulus, μ: Shear modulus

There have been several articles over the years defining the relation between density and P-wave velocity in the crust and uppermost mantle. These include Gardner's relation ($\rho = 0.23v^{0.25}$; Gardner et al., 1974), valid for a Vp range of 1.5 to 6.1 km/s; the Nafe & Drake (1957) and Ludwig et al., (1970) empirical relation, valid for a Vp range of 1.5 to 8.5 kms^{-1}; the Christensen & Mooney equation ($\rho = 0.541 + 0.3601V_p$; Christensen & Mooney 1995), valid for a V_p range of 5.5 to 7.5 km/s; and the Sobolev & Babeyko (1994) relation, valid for Vp range of 6.0 to 7.8 km/s.

In this study, the Nave & Drake (1957) and Ludwig et al., (1970) relation has been used. The reason for choosing this equation is because of its wide validity interval (1.5 – 8.5 km/s). This relation is given as:

$$\rho = 1.6612V_p - 0.4721V_p^2 + 0.0671V_p^3 - 0.0043V_p^4 + 0.000106V_p^5 \quad 4.13$$

where ρ is density and Vp is P-wave velocity.

5. METHODOLOGY

5.1 Wavelength Filtering

The term filtering can be applied to several methods in science & engineering that aim to separate anomalies on the basis of their wavelength and/or trend (Blakely et al., 1996). In order to enhance gravity anomalies and help to reveal geological and structural features, wavelength filtering has been applied. In the subsequent sections, the method of wavelength filtering which is relevant to this study is discussed.

5.1.1 Fourier transformation

Bouguer gravity anomaly (BA) contains signals from all subsurface sources. Some of the anomalies are short wavelength caused mostly by density heterogeneity in the crust. Some of the BA anomalies can be caused by deep structures and have very long wavelengths. Therefore, the Bouguer anomalies need to be filtered depending on the objective of the specific study. Wavelength filtering in the Fourier domain helps to eliminate the unwanted wavelengths in the anomalies. The method requires that the gravity data be converted into the wavenumber using a Fourier transformation (Telford et al., 1990). The Fourier transformation of a function *f* is defined as:

$$F(k_x, k_y) = \iint_{-\infty}^{\infty} f(x,y) e^{-i(k_x x + k_y y)}\, dxdy \qquad 4.14$$

The inverse Fourier transformation works the other way round and is given as:

$$f(x,y) = \iint_{-\infty}^{\infty} F(k_x, k_y) e^{i(k_x x + k_y y)}\, dk_x dk_y \qquad 4.15$$

where $k_x = \frac{2\pi}{\lambda_x}, k_y = \frac{2\pi}{\lambda_y}$ are wavenumbers

5.2 Regional-Residual Separation

5.2.1 Low pass filter

Low pass filter suppresses short wavelength anomalies of surface (crustal) origin and enhances regional long wavelength gravity anomalies of deep origin.

The low pass filter G (k_x, k_y) used in this study is given as:

$$g(k_x, k_y) = \begin{cases} 0, if\ \sqrt{k_x^2 + k_y^2} > \frac{2\pi}{\lambda_c} \\ 1,\ Else \end{cases} \qquad 4.16$$

where λ_C is the cut off wavelength. To keep the signal of interest in the interpretation, the cut off wavelength λ_C should be selected carefully.

At the end of low pass filtering the regional gravity map of the area can be obtained.

5.2.2 High pass filter

High pass filter suppresses long wavelength anomalies of deep origin and enhances short wavelength gravity anomalies of shallow origin. As in the case of low pass filter, selection of the cut off wavelength is critical.

The high pass filter G (k_x, k_y) used in this study is given as:

$$G(k_x, k_y) = \begin{cases} 0, if \sqrt{k_x^2 + k_y^2} < \frac{2\pi}{\lambda_c} \\ 1, \ Else \end{cases} \quad 4.17$$

5.3 Upward Continuation

Upward continuation is a mathematical projection of data measured on the surface to a higher elevation (Figure 8, top). This process is based on the physical fact that the more distant the observation is from the body causing the anomaly, the broader or longer the wavelength of the anomaly. Upward continuation is a filter that smooths the gravity anomaly measured on the surface by attenuating the short wavelength anomalies relative to the long wavelength counterparts.

The upward continuation filter is defined as:

$$G(k_x, k_y) = e^{-kZ} \quad 4.18$$

where $k = \sqrt{k_{x^2} + k_{y^2}}$ $k_x = \frac{2\pi}{\lambda_x}, k_y = \frac{2\pi}{\lambda_y}$ are wavenumbers and z is the height of continuation.

5.4 Downward Continuation

Downward continuation is a process by which potential field data is mathematically projected downward from one datum to a level surface below the datum (Figure 8, bottom). Downward continuation sharpens the anomalies measured at the surface.

The downward continuation filter is given as:

$$G(k_x, k_y) = e^{+kZ} \quad 4.19$$

where $k = \sqrt{k_{x^2} + k_{y^2}}$ $k_x = \frac{2\pi}{\lambda_x}, k_y = \frac{2\pi}{\lambda_y}$ k_x and k_y are wavenumbers and z is the height of continuation.

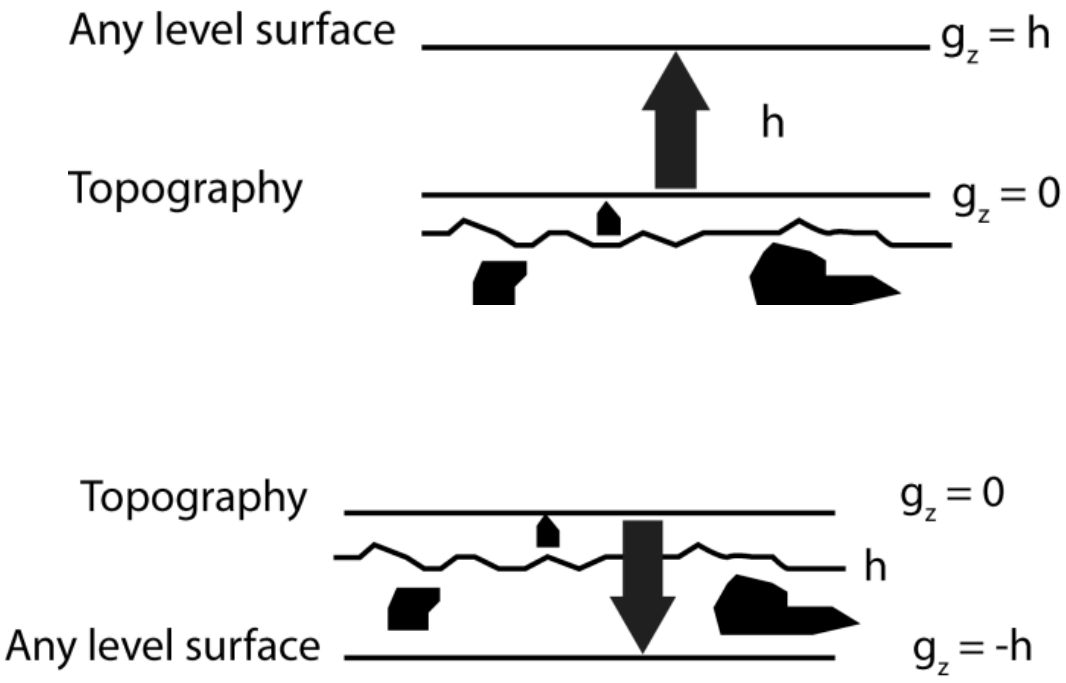

Figure 8. (Top): Upward and (**bottom):** downward continuation concept.

5.5 Gravity Data Modeling

There are various methods available to perform gravity data modeling. They can generally be categorized as forward and inverse modeling (Figure 9).Both forward and inverse problems are inherently non-unique and need well constrained data.

5.5.1 Forward modeling

The forward modeling technique begins with the establishment of a model based on geological and geophysical perception. Based on the initial model, gravity anomalies are calculated. The calculated anomalies are compared with observed gravity data, and the model is adjusted until the predicted data fit the observed data (Blakely et al., 1996).

5.5.2 Inverse modeling

Inverse modeling (inversion) uses data to infer the form and physical parameters of a causative body (i.e. density, shape, and maximum depth). The Inverse problem is inherently non-unique and needs well constrained data (Blakely et al., 1996).

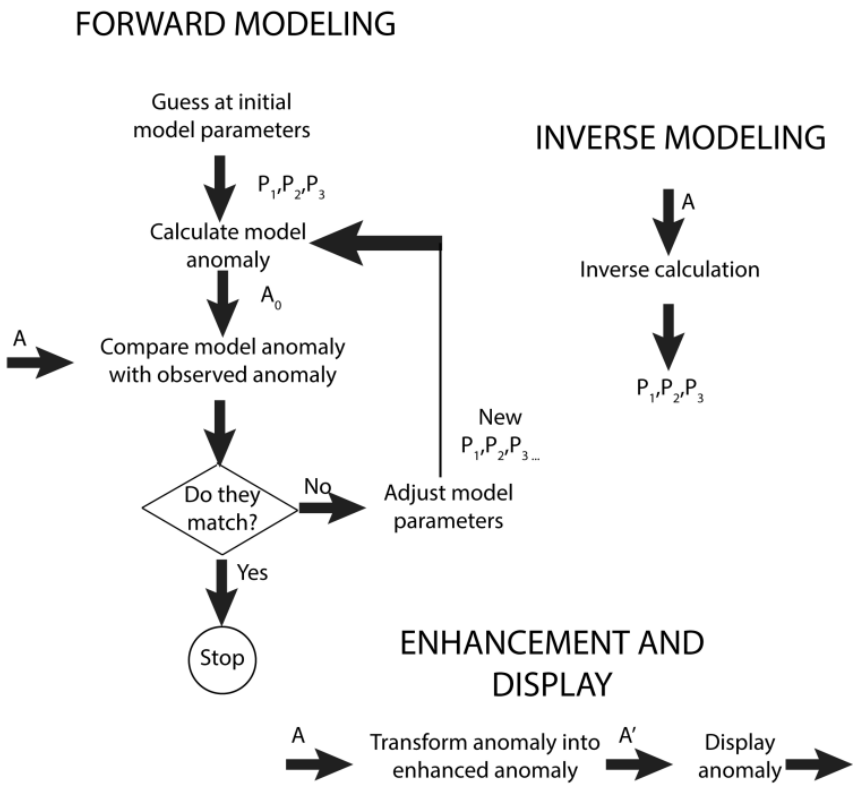

Figure 9. Techniques of potential field data interpretation. The measured anomaly is represented by A, calculated anomaly by A0, and transformed anomaly by A'. Parameters P1, P2, P3 are attributes of the source (Modified after Blakely et al., 1996).

5.5.3 2-D Forward Modeling

The dimensionality of potential filed modelling depends on the assumed length of tectonic structures along strike (Figure 10). A 2-dimensional model may be visualized as a number of tabular prisms with their axes perpendicular to the strike; blocks and surfaces are presumed to extend to infinity in the strike direction (Figure 10a). It is possible to derive the gravity anomaly associated with an irregular shape by simplifying it to a many sided prism or polygon. It is assumed that the vertices of an n sided polygon can be described as ABCDEF (Figure 11). The point P is the origin of an xz coordinate system and the polygon lies in the xz plane.

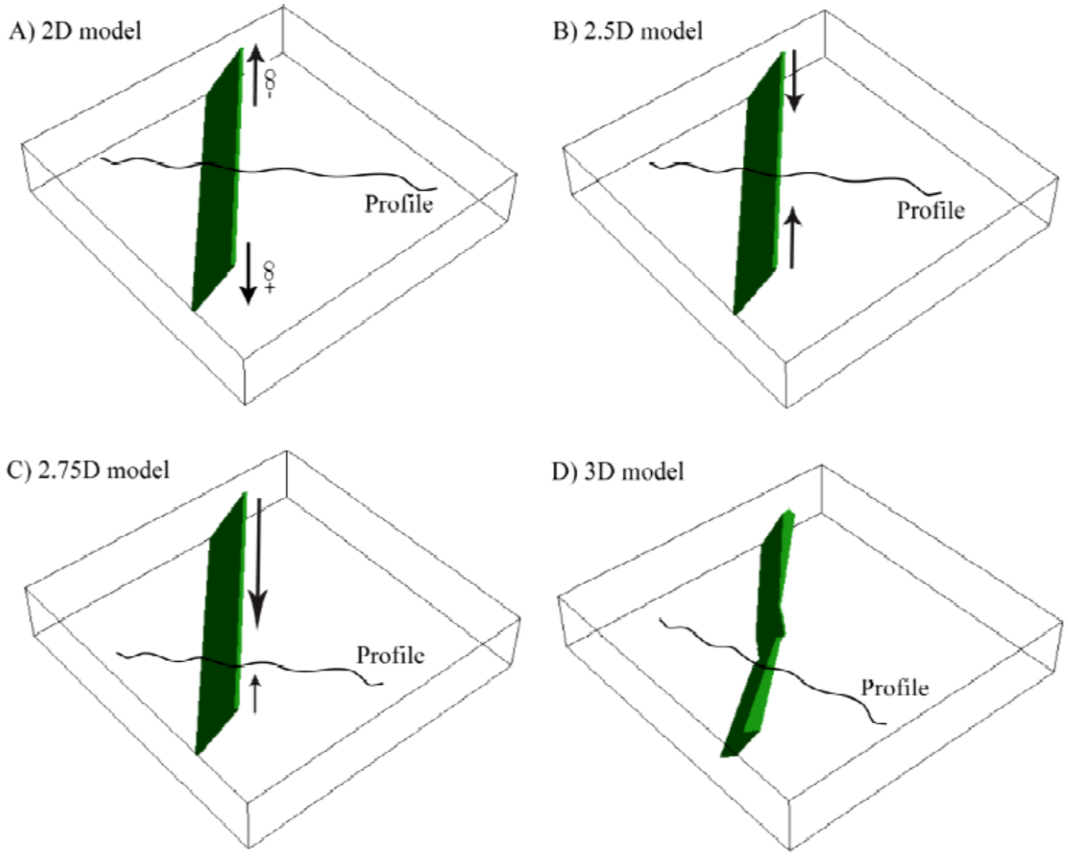

Figure 10. Schematic representations of dimensionality in potential field modeling (from Malehmir 2007).(A) 2D, infinite strike length, (B) 2.5D, finite strike length, (C) 2.75D, finite and asymmetric strike length and (D) 3D, considers 3D structural shapes in space.

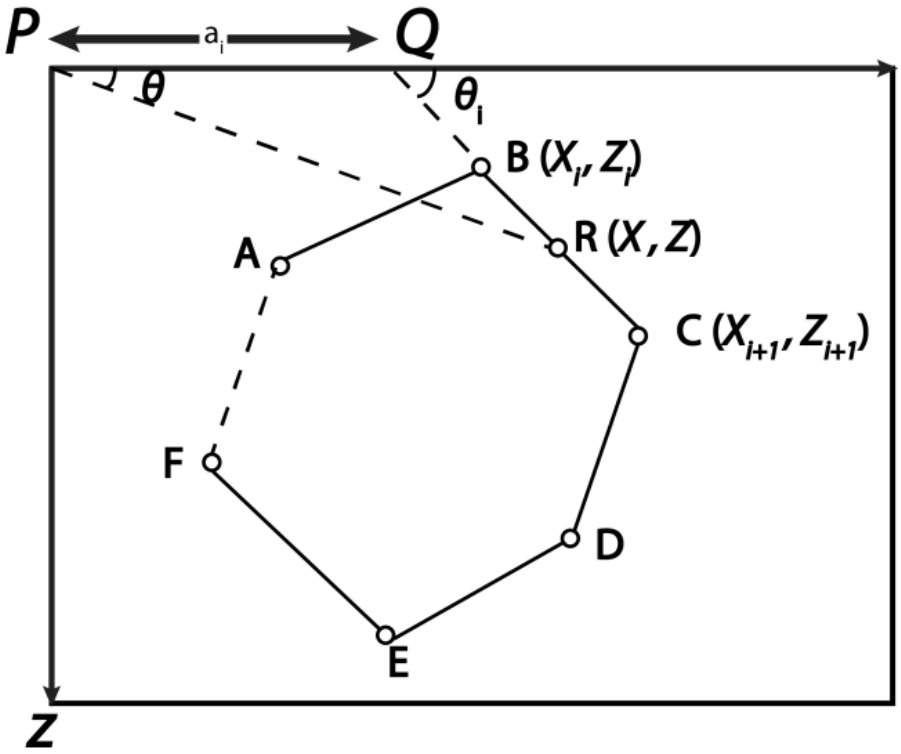

Figure 11. Geometrical elements involved in the gravitational attraction of an n-sided polygon (modified after Talwani et al., 1959). *z*, defined as positive downwards (vertical); θ, measured from the positive *x* axis towards the positive *z* axis; *G*, is the universal constant of gravitation; *p* is the volume density of the body.

The vertical component of the gravitational attraction due to a two-dimensional body is given as (Hubbert, 1948):

$$gv = 2Gp \oint z \, d\theta \qquad 4.20$$

where G is the universal gravitational constant and p *is density*.

The corresponding expression for the horizontal component of gravitational attraction is given by $\mathrm{gh} = 2Gp \oint x \, d\theta$.

Considering PQ = a_i and $z = x \tan\theta = (x - a_i) \tan\phi_i$, the expression of z for any arbitrary point R on BC takes the following form:

$$Z_i = \frac{a_i \tan\theta \ \tan\phi_i}{\tan\phi_i - \tan\theta} \qquad 4.21$$

The summation of Z_i and H_i over the n sides of the polygon results in:

$$Z_i = a_i \sin\emptyset_i cos\,\emptyset_i \left[\theta_i - \theta_{i+1} + tan\emptyset_i \log\frac{\cos\theta_i(\tan\theta_i - \tan\emptyset_i)}{\cos\theta_{i+1}(\tan\theta_{i+1} - \tan\emptyset_i)}\right] \qquad 4.22$$

$$X_i = a_i \sin\emptyset_i cos\,\emptyset_i \left[\tan\emptyset_i(\theta_{i+1} - \theta_i) + \log\frac{\cos\theta_i(\tan\theta_i - \tan\emptyset_i)}{\cos\theta_{i+1}(\tan\theta_{i+1} - \tan\emptyset_i)}\right] \qquad 4.23$$

where $\theta_i = \tan^{-1}\frac{z_i}{x_i}$ and $\emptyset_i = \tan^{-1}\frac{z_{i_{+1}} - z_i}{x_{i_{+1}} - x_i}$

Thus, the vertical and horizontal components of gravitational attraction due to a polygon are given, respectively as:

$$V = 2G\rho\sum_{i=1}^{n} Z_i\,, \qquad H = 2G\rho\sum_{i=1}^{n} X_i$$

where ρ is the density of the body and G is the universal gravitational constant.

The gravity profiles for this study are modeled using GM-SYS, which computes the gravitational attraction of multiple two dimensional polygonal bodies with finite strike lengths (2.5D). The computation of the gravity response of the two-dimensional sources is based on Talwani's method (Talwani et al., 1959; Talwani and Heirtzler, 1964). GM-SYS uses a two-dimensional flat-earth model to calculate gravity and magnetic responses. Each structural unit or block extends to a finite length perpendicular to the profile (along strike). The earth is assumed to have topography but no curvature. The 2.5-D models are extended to 30,000 kilometers along the profile to eliminate edge effects (GM-SYS User Manual, 2006).

5.5.4 3-D Modeling (Parker's Method)

Most of the 3-D gravity modeling algorithms that are used to calculate the gravity response of 3-D bodies involve indefinite volume integrals and are computationally intensive. In these cases, the method introduced by Parker et al., (1972) simplifies 3-D gravity modeling procedures and save computational time. Moreover, the terrain effect is minimized in 3-D modeling.

The Parker's method provides the gravity response of a layered earth model with variable densities from known topography in the Fourier domain or vice versa.

The relation between topography and gravity in Fourier domain is defined as:

$$F(\Delta g) = -2\pi G\rho \exp(-\left|\vec{k}\right|z_0) \sum_{n=1}^{\infty} \frac{\left|\vec{k}\right|^{n-1}}{n!} F[h^n(r)] \qquad 4.24$$

$r = (x, y, z)$ represents the position in space

where $F(\Delta g)$ is the Fourier transform of the gravity anomaly, G is the gravitational constant, ρ is the density contrast across an interface, k is the wave number, $F(h(r))$ is the Fourier transform of the depth to an interface (positive downwards) and z_0 is the mean depth of a horizontal interface.

6. GRAVITY DATABASE

The gravity models presented in this study are based on combined satellite and terrestrial gravity data from the European Improved Gravity Model (EIGEN-6C2; Förste et al., 2012). The EIGEN-6C2 is a high-resolution global gravity field model up-to degree and order of 1949. It is based on the WGS84 reference system. The spatial resolution of this model is ~10 km. It is the first combined model that includes satellite gravity data from GOCE (Gravity field and steady-state Ocean Circulation Explorer), GRACE (Gravity Recovery and Climate Mission) and LAGEOS (Laser Geodynamics Satellites) satellite missions. In addition to the standard gravity data corrections, the gravity data from the EIGEN-6C2 model is reduced using an infinite slab for Bouguer correction term with densities 2.670 g cm^{-3} onshore and 1.645 g cm^{-3} offshore. In the following subsequent sections, the components of the EIGEN-6C2 model are described.

6.1 Satellite Data

GRACE (Gravity Recovery and Climate Mission)

The first GRACEs (twin satellites in orbit, ~220 km apart) were operational from March 2003 to December 2010. The twin satellites, those were on the same orbit above the Earth, provided gravity data from 460 km altitude (Figure 12). On the orbit, one of the twin satellites leads the other. When the leading satellite detects an increase in gravitational pull, it speeds up and hence the distance from the other twin satellite increases. Conversely, when the leading satellite passes over an area of slightly weaker gravity, it slows down and consequently the

distance between the two satellites decreases. The change in gravity is related to the change in distance between the satellites. The changes in distance between the twin satellites are determined using two way travel time of microwave pulses.

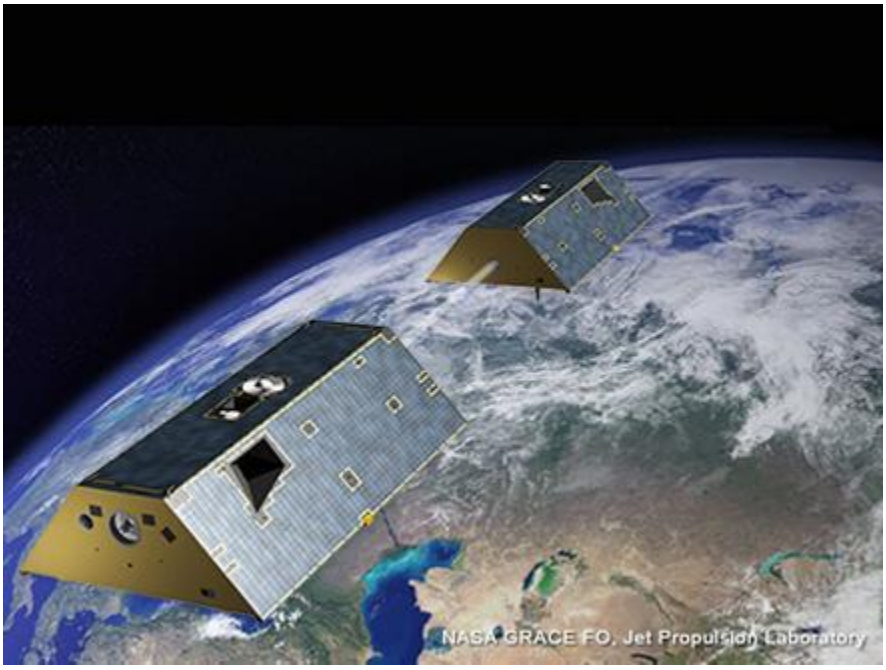

Figure 12. Twin satellites of GRACE mission (from http://www.jpl.nasa.gov/missions/gravity-recovery-and-climate-experiment-grace/).

GOCE (Gravity field and steady-state Ocean Circulation Explorer)

GOCE was operational from Nov 1, 2009 to April 19, 2013. The satellite had three pairs of accelerometers and measured slight changes in acceleration due to variations in gravity (~1 mgal) (www.esa.int/esaLP/LPgoce.html). In contrast to GRACE and LAGEOS, GOCE provided full tensor gravity gradient data from 250 km altitude.

The GOCE gradiometer contains three pairs of proof masses positioned at the outer ends of three 50 cm long orthogonal arms (Figure 13). Because of their different position in the

gravitational field they all experience the gravitational acceleration of Earth slightly differently. The three axes of the gradiometer allow the simultaneous measurement of six independent but complementary components of the gravity field.

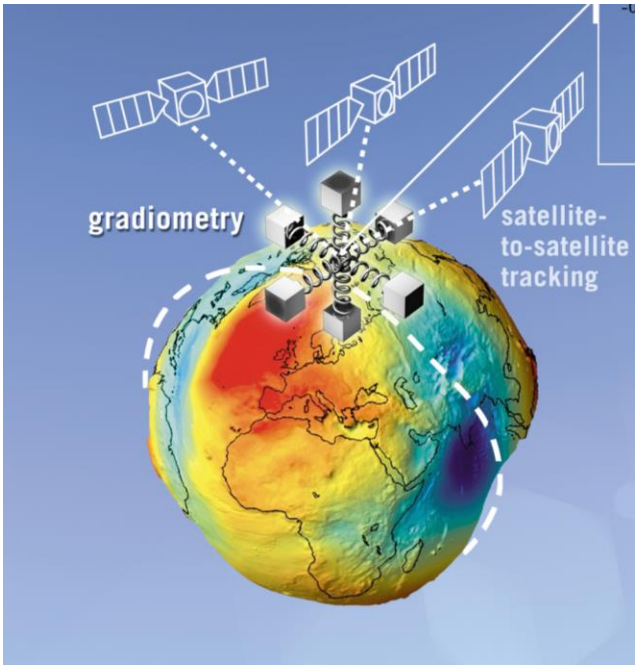

Figure 13. GOCE satellite mission including gradiometer (from http://www.esa.int/spaceinimages/Images/2008/06/GOCE_takes_six_simultaneous_measurements_of_the_gravity_field).

LAGEOS (Laser Geodynamics Satellites)

LAGEOS (SLR) was operational from January 1985 to December 2010 and its data has been used as a part of the EIGEN-6C2 model.

6.2 Surface Data

The surface data over the oceans and lands are from the altimetry-derived gravity anomalies and the Earth Gravitational Model (EGM2008), respectively (Andersen et al., 1998;

Pavlis et al., 2012). The Bouguer anomaly map of the Aegean and Anatolian regions is shown in Figure 14. The gravity anomaly map has been obtained from EIGEN-6C2 model.

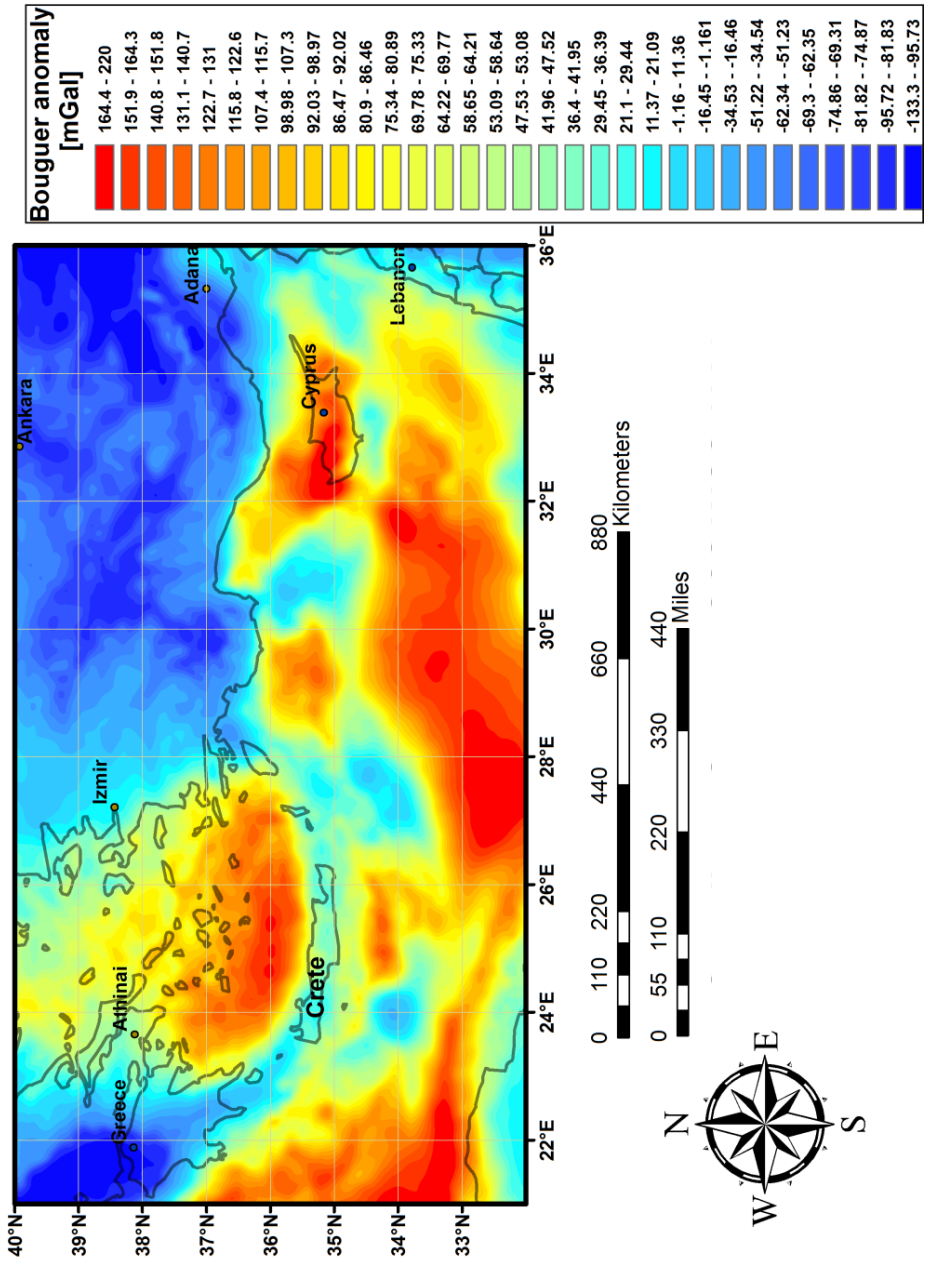

Figure 14. Bouguer gravity map of the Aegean-Anatolian region from combined satellite and terrestrial gravity data. The gravity data are from the European Improved Gravity model of the Earth (EIGE-6C2; Förste, et al., 2012).

7. RESULTS AND DISCUSSIONS

7.1 Regional-Residual Separation

In the following sections, the results of the regional-residual separation of gravity anomalies and their interpretation in terms of magmatic centers and crustal structures are discussed. As discussed in section 5.2, the anomalies are separated using wavelength filtering. The low-pass (long wavelength) filter suppresses short wavelength anomalies of shallow origin and enhances regional long wavelength gravity anomalies of deep origin. The high-pass (short wavelength) filter suppresses long wavelength anomalies of deep origin and enhances short wavelength gravity anomalies of shallow origin. The cut-off wavelength (300 km) has been selected based on the similarity of amplitudes of gravity anomalies obtained using an upward continuation and wavelength filtering.

7.1.1 Upward continued maps

Upward continuation is a process by which potential field data are mathematically projected upward from one datum (usually surface) to a level surface above the datum to enhance the long wavelength components of the Bouguer anomalies. Thus, the process is equivalent to a low pass filter.

To suppress the high frequency signals related to near surface bodies, the Bouguer gravity anomalies have been projected upward to various heights (30 km, 40 km, 50 km and

above).It was found that upward continuation of the gravity field to a height of 50 km suppresses short wavelength anomalies of shallow origin and results in a regional field (Figure 15 a,b,c).

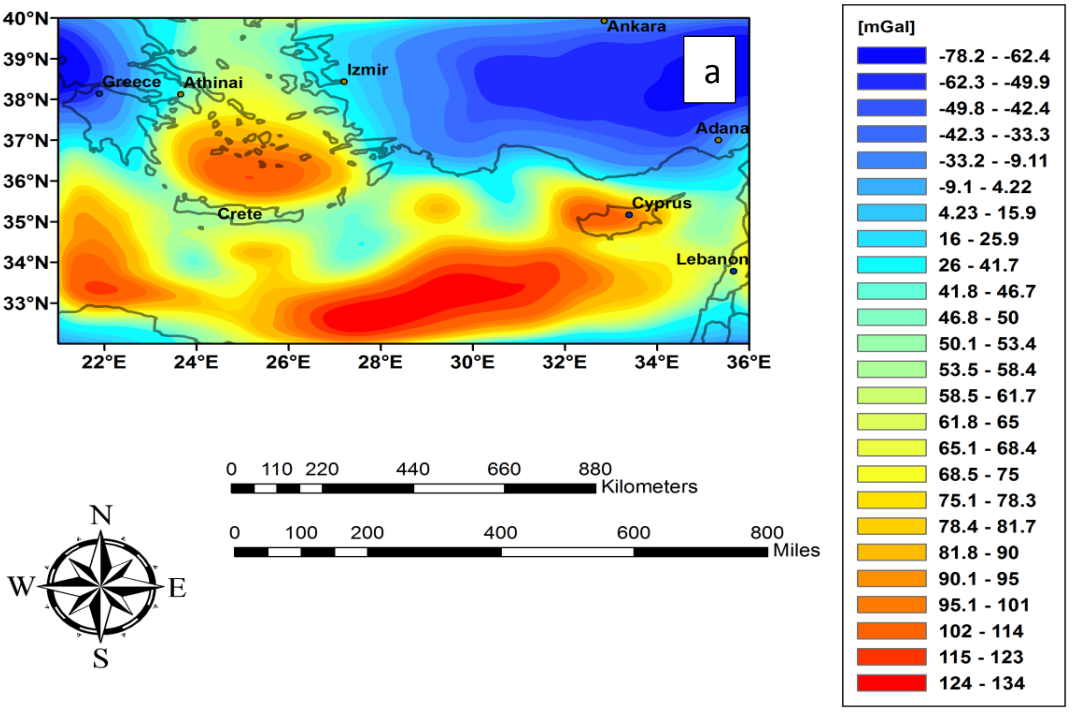

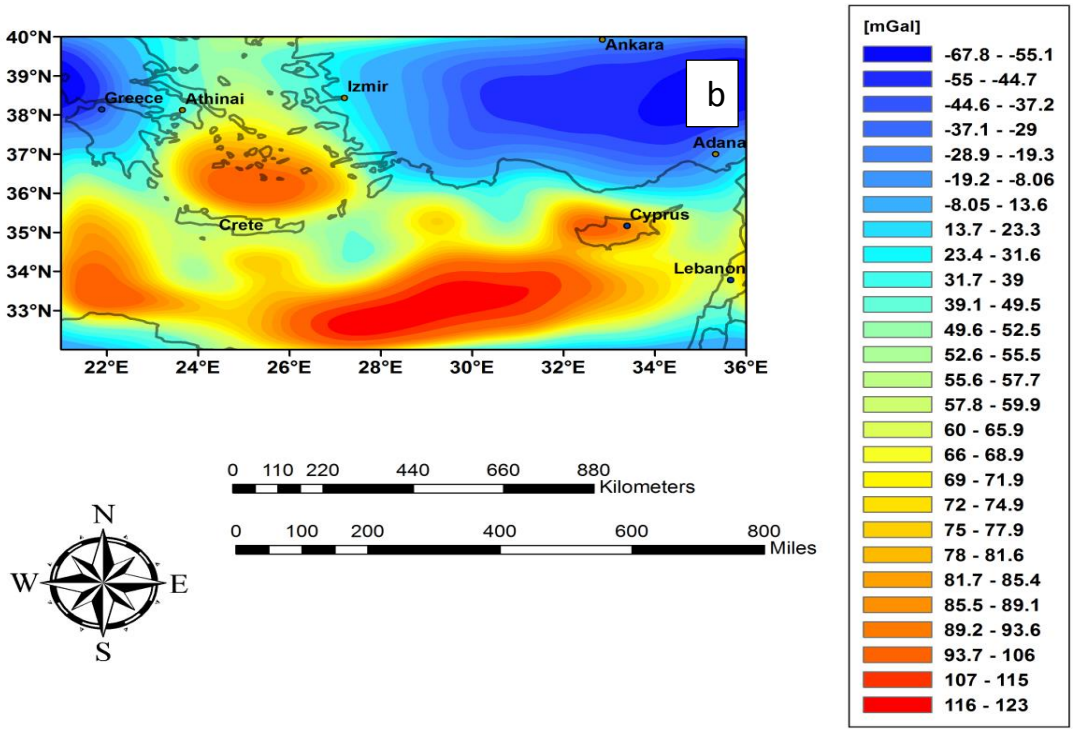

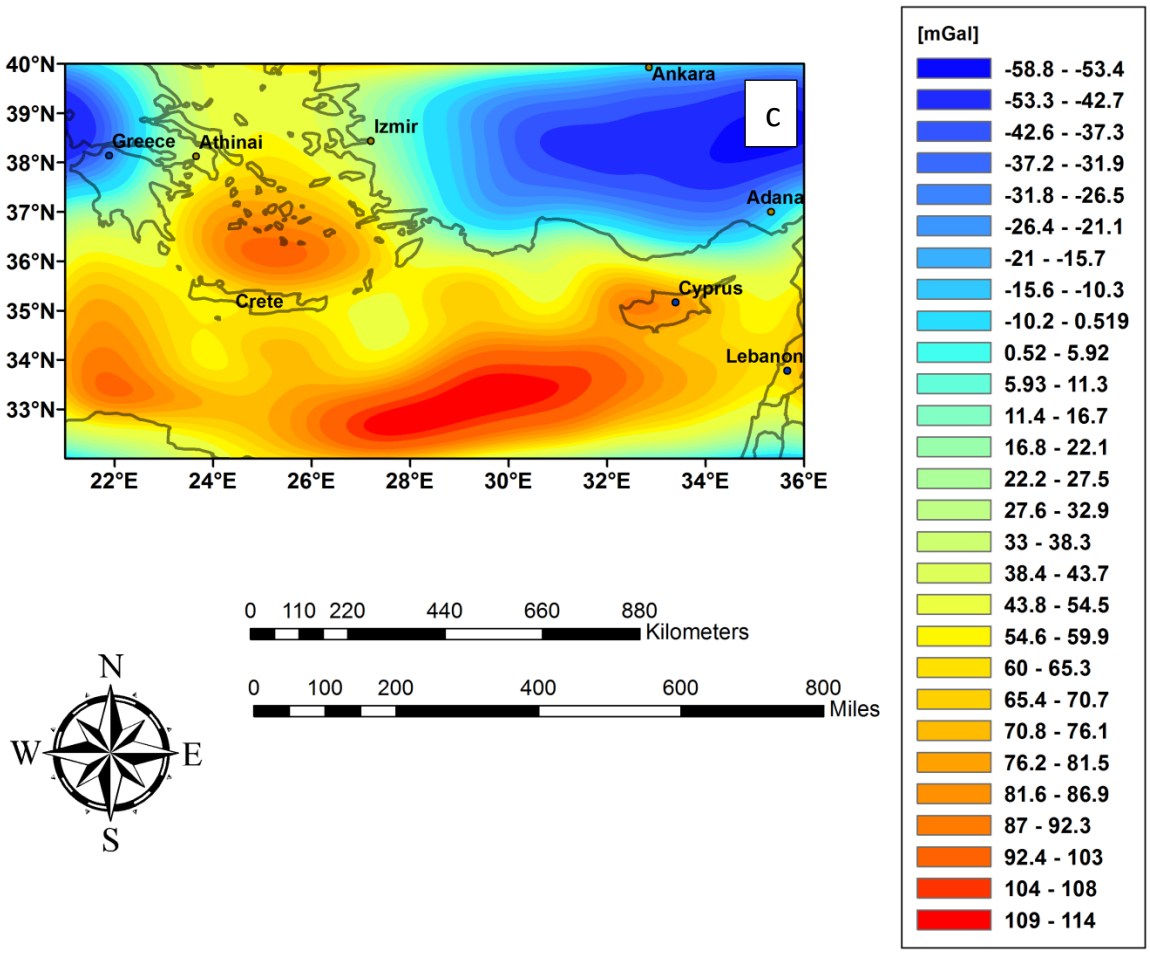

Figure 15 a,b,c. Upward continued maps of the Aegean-Anatolian region at heights of 30 km, 40 km and 50 above topography, respectively.

7.1.2 Residual gravity anomalies

The residual gravity map shows anomalies ranging from -124 mGal to 136 mGal (Figure 16). The northwestern part of Greece, Crete, and the southern boundary of Anatolia are characterized by low residual gravity anomalies (~-124 mGal). The low residual gravity anomalies can be related to Cenozoic sediments. The northern part of the study area (north of Izmir) also exhibits a low residual gravity anomaly that can be related to the Izmir-Ankara-Eskisehir suture zone between Sakarya and the Istanbul lithospheric terranes.

The positive residual anomalies of the study area might be associated with the volcanic arcs of the Hellenic and Cyprus subduction zones and volcanic fields in western Anatolia (e.g. Kula volcanic field KVF, Kirka-Afyon-Isparta volcanic field KAIVF; Figure 1). The KVF and KAIVF are associated with the alkaline volcanism of Pliocene to Middle-late Miocene (Richardson-Bunbury 1996; Savaşçın and Oyman 1998; Dilek and Altunkaynak 2009). Various geochemical studies indicate that the volcanism in the region is associated with rapid asthenosphere upwelling beneath western Anatolia (Gülen et al., (1990); Tokçaer et al., (2005); (Prelević et al., 2012). Therefore, the positive patchy residual Bouguer anomalies may be related to accretion of denser asthenospheric material on to the crust.

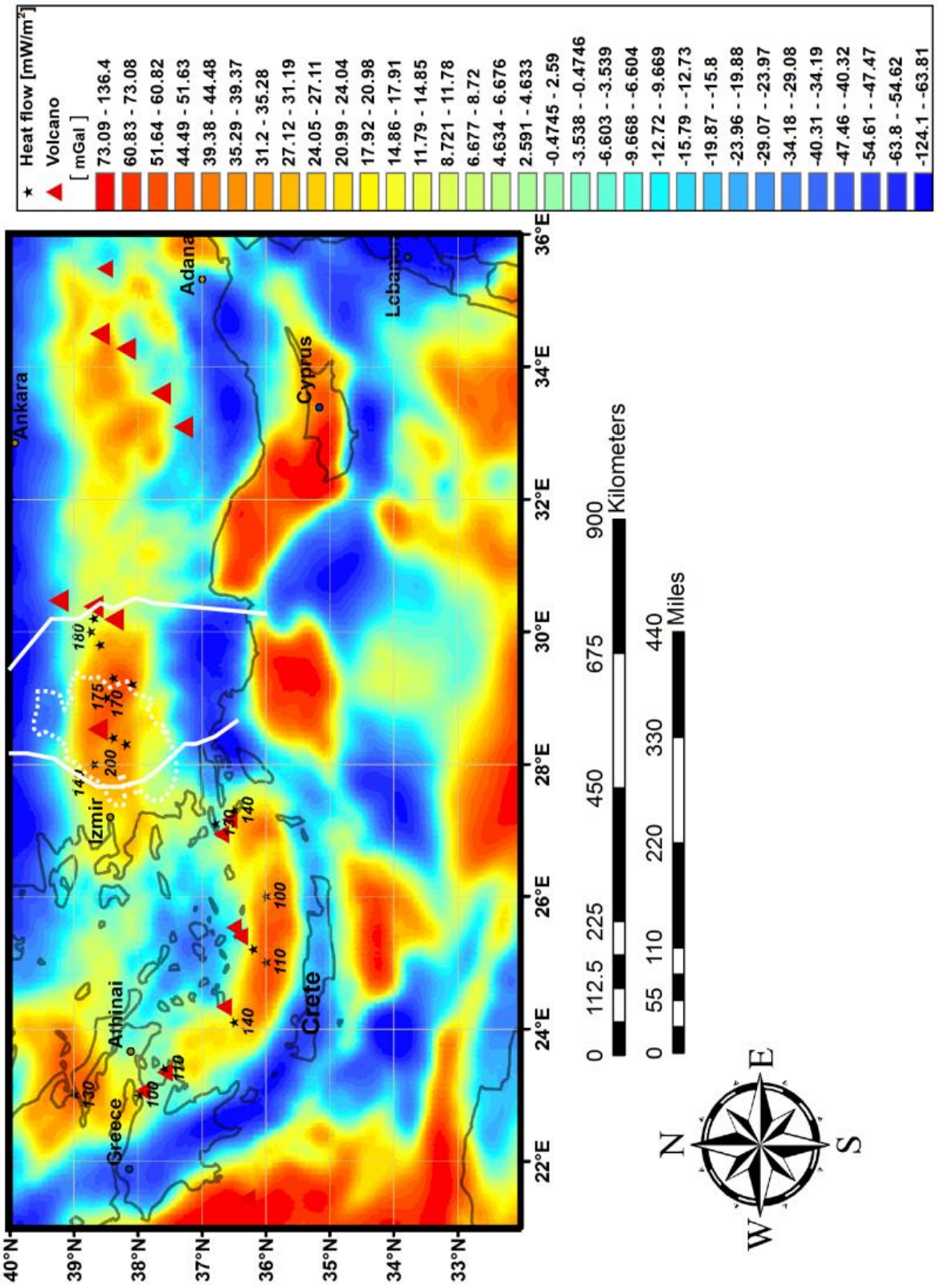

Figure 16. Residual anomaly map of the Aegean-Anatolian region. White dashed line shows the Menderes Massif Complex. Solid white line represents the asthenospheric window area defined by seismic tomography (Biryol et al., 2011). Red triangles and black small stars are for volcanoes and heat flow, respectively (Akin et al., 2014).

7.1.3 Regional gravity anomalies

Unlike the residual anomaly map, the regional gravity anomaly map (Figure 17) shows a regional trend similar to the Bouguer anomaly map (Figure 14) over the study area. The regional gravity anomalies increase from central Anatolia towards the north and south (Figure 17). The gravity values in the regional map vary from -119 mGal to 165 mGal (Figure 17). The positive regional gravity anomalies north of Crete might be related to magmatic centers (volcanoes). The northwestern part of Greece shows low regional values.

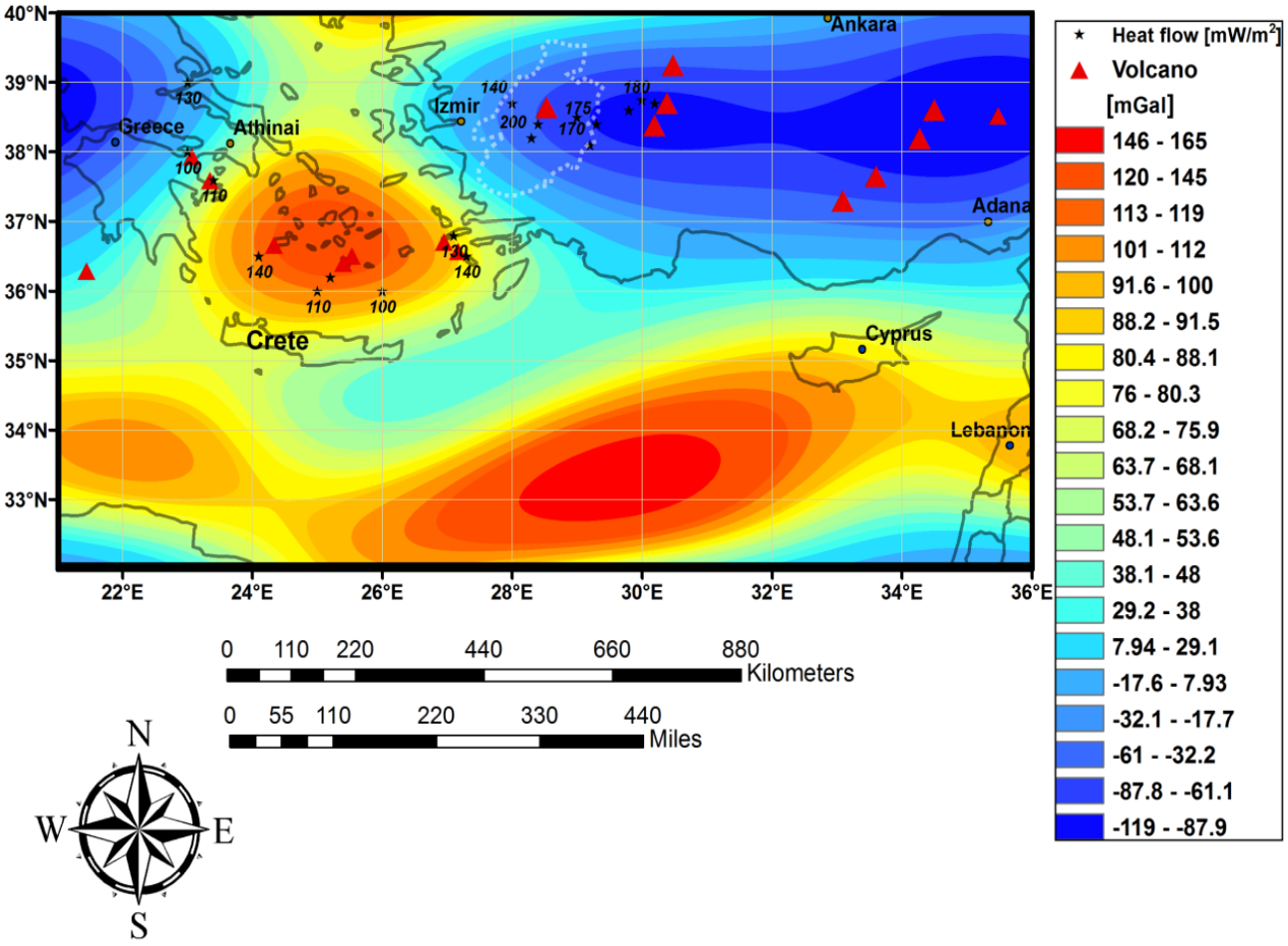

Figure 17. Regional anomaly map of the Aegean-Anatolian region. White dashed line shows the Menderes Massif Complex. Red triangles and black small stars show volcanoes and heat flow, respectively (Akin et al., 2014).

7.2 Gravity Models

7.2.1 Initial model and constraining data

To establish the crust and upper mantle structure of the Aegean-Anatolian region, 2.5-D gravity models were developed along seven profiles perpendicular to the Hellenic and Cyprus trenches. The profiles extend from 34°N to 40°N latitude. One profile was selected to cross the Crete and Hellenic subduction zone at 24°E; two profiles cover the western and eastern edges of the asthenospheric window area along 27°E and 31°E, respectively; three profiles (28.5°E, 29°E and 29.5°E) are selected to cover the asthenospheric window area outlined by seismic tomography (Biryol et al., 2011; Salaün et al., 2012; Gessner et al., 2013), the asthenospheric window area includes the Menderes Massif Complex; and two profiles that extend from Cyprus to central Anatolia along 31°E and 33°E. For the purpose of discussion, the profiles are grouped based on their locations: Aegean (P1 and P2 at 24°E and 27°E, respectively; Figure 1); southwestern Anatolia (P3, P4 and P5 at 28.5°E, 29°E and 29.5°E, respectively: Figure 1); and Cyprus (P6 and P7 at, 31°E and 33°E, respectively; Figure 1).

The initial geometry of the Hellenic and Cyprus slab in the 2.5-D model was based on earthquake hypocenter determination and seismic tomography (Spakman et al., 1988, 1993; Papazachos and Nolet, 1997; Bijwaard et al., 1998; Piromallo and Morelli, 2003; Schmid et al., 2004; Chang et al., 2010; Biryol et al., 2011; Salaün et al., 2012; Gessner et al., 2013). The earthquakes data are from Boğaziçi University include events from 1980 to 2015 (http://udim.koeri.boun.edu.tr/zeqdb/indexeng.asp).

The densities of the Hellenic and Cyprus slabs were constrained by results of seismic tomography studies (Wortel and Spakman, 2000; Papazachos et al., 2000; Piromallo and Morelli, 2003; Endrun et al., 2005; van Hinsbergen et al., 2010; Biryol et al., 2011; Salaün et al., 2012). The velocities have been converted to densities using Nafe and Drake relation (Nafe and Drake (1957).

The densities and thicknesses of the upper crust (8 – 20 km) and the Moho depth (20 – 55 km) for the overriding plate have been obtained from several previous studies (Saunders et al., 1998; Zhu et al., 2006; Akyol et al., 2006; Tezel et al., 2007; Di Luccio et al., 2007; Di Luccio & Pasyanos, 2007; Çakır and Erduran, 2011; Mutlu and Karabulut, 2011; Ates et al., 2012; Tezel et al., 2010, 2013; Vanacore et al., 2013; Karabulut et al., 2013; Sayil et al., 2014; Salah et al., 2014; Kind et al., 2015). The density values for each tectonic unit in the gravity model are shown in Table 1.

Sediment thickness in the Aegean-Anatolian region varies from 4 to 18 km (Makris and Yegorova, 2006; Sari et al., 2006; Akyol et al., 2006; Casten et al., 2006; Zhu et al., 2006; Di Luccio et al., 2007; Snopek et al., 2007; Işık et al., 2009; Tezel et al., 2013; Makris et al., 2013; Sayil et al., 2014). These values are used to constrain the sediment thicknesses in the 2.5-D gravity model of this study.

Table 1. Tectonic units of the gravity model and their respective densities

Tectonic units	**P wave velocity (km/sec)**	**Density (g/cm^3)**	**References**
Sediment	4.5-5.7	2.45-2.65	Saunders et al., (1998); Zhu et al., (2006); Çifçi et al., (2011); Salah et al., (2014); Sayil et al., (2014); Welford et al., (2015)
Upper crust	5.90-6.2	2.70-2.75	Bohnhoff et al., (2001); Endrun et al., (2005); Meier et al., (2004,2007); Akyol et al., (2006); Salah et al., (2014); Makris et al., (2013); Tezel et al., (2010,2013);
Lower crust	6.35-6.95	2.80-2.95	
Mantle	7.75-8.00	3.20-3.30	Endrun et al., (2005); Nikolingata et al., (2007); Biryol et al., (2011); Makris et al., (2013); Salah et al., (2014)
Oceanic crust	6.75-8.30	2.90-3.40	Endrun et al., (2005); Makris et al., (2010,2013)
Oceanic lithosphere	7.75-8.30	3.20-3.40	Endrun et al., (2005); Makris et al., (2010,2013)
Low- velocity asthenospheric material	7.95	3.12 - 3.27	Biryol et al., (2011)
Asthenosphere	8.35	3.42	Endrun et al., (2005); Makris et al., (2013); Sayil et al., (2014);

7.2.2 Structure of the Hellenic Arc

Figure 18 shows a 2.5-D gravity model of the crust and upper mantle structure of the Aegean region. The profile is 710 km long and extends from 34°N to 40°N. The depth to the bottom of the model is 165 km. The Bouguer gravity anomaly along the profile varies from -25 mGal to 141 mGal. The model consists of water, sediment, upper crust, lower-crust, the Hellenic slab (oceanic crust and lithosphere), continental lithosphere and the asthenosphere.

The model shows the subduction of the Hellenic slab beneath the Aegean region. The angle of subduction of the Hellenic slab, as predicted from gravity modeling and constrained by earthquake hypocenters, is ~40°, and this is in agreement with results of seismic tomography (40°-50° ; Wortel and Spakman, 2000; Biryol et al., 2011). However, some previous studies predicted a flat slab in this region (20°–30°; Li et al., 2003; Sodoudi et al., 2006; Bakırcı et al., 2012). The different results may be attributed to differences in resolution of the various tomography models.

The crustal thickness beneath Crete, as predicted from gravity modeling, is ~33 km, and this is consistent with the previous crustal thickness determination in the region (~ 32 km; Bohnhoff et al., 2001; Li et al., 2003; Endrun et al., 2005; Casten et al., 2006; Meier et al., 2007 Makris et al., 2013). The Moho depth beneath eastern Greece and the Peloponnese peninsula varies from 32 to 40 km, which is in a range determined by Karagianni et al., (2005), Sodoudi et al., (2006), Di Luccio et al., (2007), Suckale et al., (2009), and Sodoudi et al., (2015). The gravity model predicts sediment thickness of 4 to 11 km beneath western Crete.

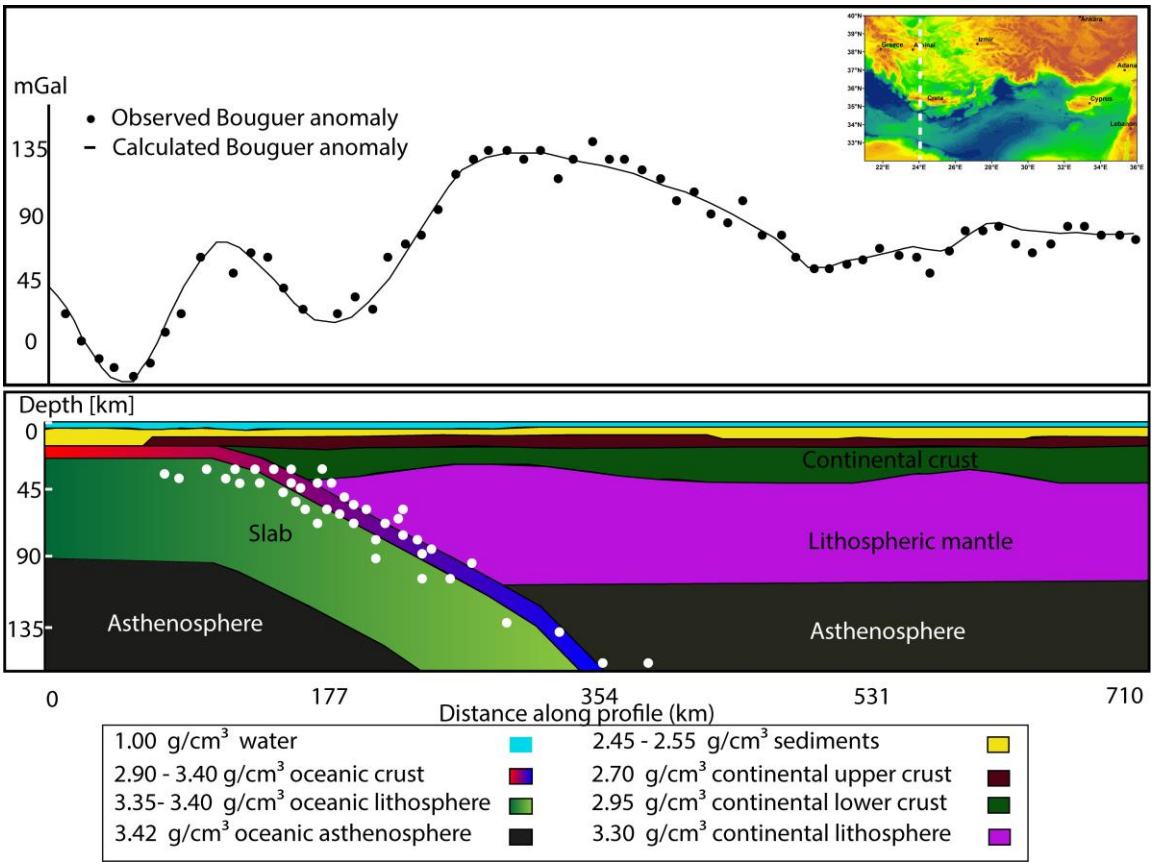

Figure 18. A 2.5-D gravity model of the Aegean region at 24°E. The location of the profile is shown in Figure 1. The white circles are earthquake hypocenters.

Figure 19 shows the crust and upper mantle structure of the eastern edge of the Hellenic arc at 27°E. This model has the same length, depth and tectonic units as in Figure 18. The Bouguer gravity anomaly along this profile varies from -13 mGal to 147 mGal. The dip of the slab, as determined from earthquake hypocenters, is ~50°.

The Moho depth varies from 25 to 30 km, which is consistent with the trend of decreasing Moho thickness in central Aegean and western Anatolia (Zhu et al., 2006, Di Luccio et al., 2007, Mutlu and Karabulut 2011, Vanacore et al., 2013, Tezel et al., 2013, Karabulut et al.,

2013).The upper and lower crustal thicknesses range from 6 - 12 km and 11 - 19 km, respectively.

Sediment thickness generally decreases from south to north, and the sediment accumulation in western Anatolia is ~3 km.

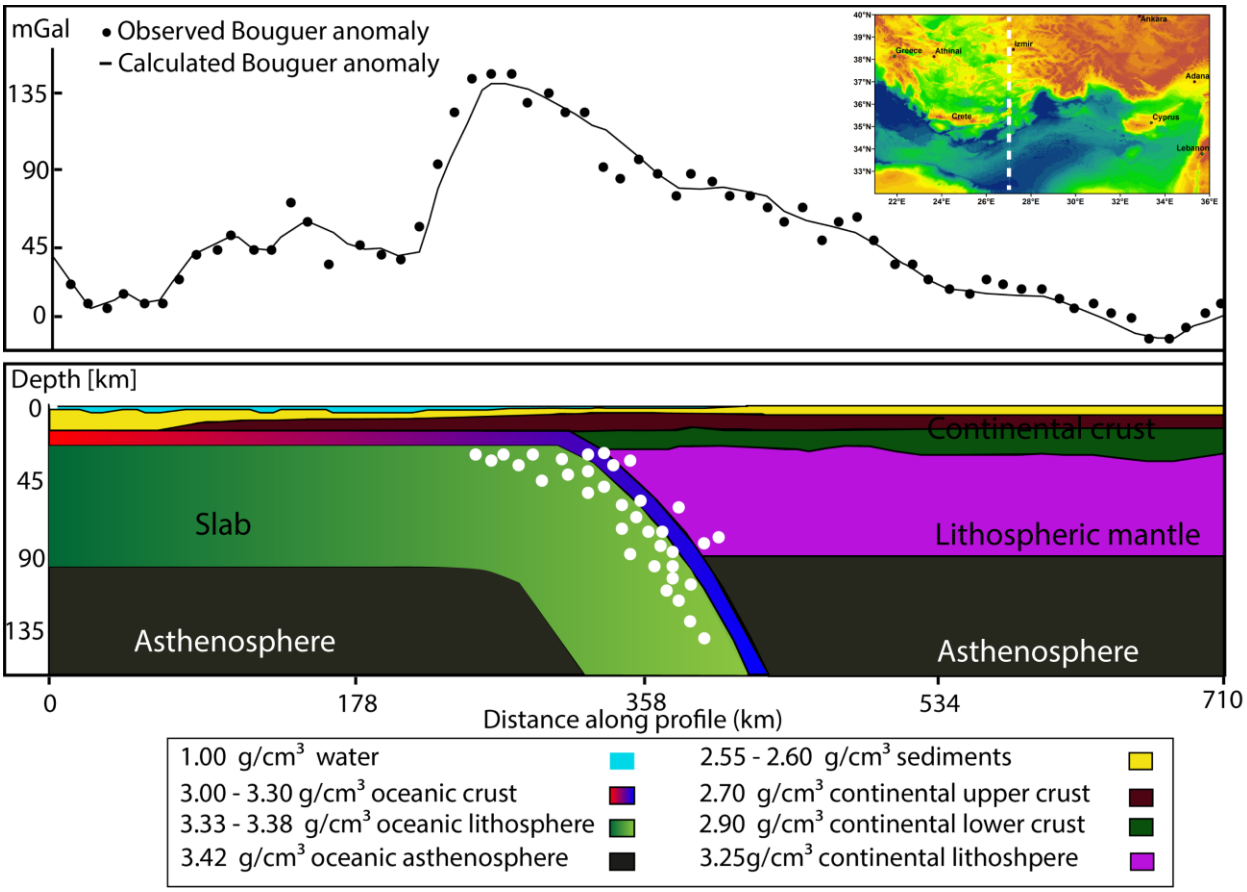

Figures 19. A 2.5-D gravity model of the Aegean region at 27°E. The location of the profile is shown in Figure 1. The white circles are earthquake hypocenters.

7.2.3 Structure of Western Anatolia

One of the objectives of this study is to assess the effect of la ow-velocity zone on crustal structures in southwestern Anatolia. The existence of a low-velocity zone in the upper mantle beneath southwestern Anatolia was reported in several seismic tomography studies (e.g. Biryol et al., 2011; Salaün et al., 2012). The low-velocity zone is interpreted as slab-tear (asthenospheric window) in the subducting African plate (Spakman et al., 1993; De Bordeer et al., 1998; Piromallo and Morelli, 2003; Biryol et al., 2011; Salaün et al., 2012).

In order to determine the effect of the low-velocity zone on the neotectonics in southwestern Anatolia, the crust and upper mantle structure of the region has been modeled along three profiles (P3, P4 & P5 at 28.5°E, 29°E and 29.5°E, respectively; Figure 1). One of the profiles (P3 at 29°E), depicting the crust and upper mantle structure of the asthenospheric window area beneath southwestern Anatolia, is shown in Figure 20. The Bouguer gravity anomaly along this profile varies from -76 mGal to 130 mGal. The Bouguer gravity anomaly along this profile is well explained in terms of a partly subducted African slab and upwelling asthenosphere beneath southwestern Anatolia (Figure 20). The dip of the slab, as obtained from gravity modeling and constrained by earthquake hypocenters, is ~15°. This is in good agreement with results from high-resolution surface wave tomography (~20°; Salaün et al., 2012). The earthquake catalog of this region shows no deep earthquakes in the asthenospheric window area. This may indicate that the subducting African slab has experienced a major slab-tear beneath southwestern Anatolia, and the gap in the slab may be a channel through which asthenospheric material is rising up to the uppermost mantle. The slab-tear is attributed to the differential trench retreat rates between the Hellenic and Cyprus trenches. The rate of retreat of the Hellenic trench

is much faster than the Cyprus trench (~30 mm/yr. and <10 mm/yr. respectively; McClusky et al., 2003; Wdowinski et al., 2006).

As shown in Figure 20, the crust above the low-velocity zone (asthenospheric window) is thinner (24 – 34 km) than the surroundings. The crustal thinning may be attributed to the hot asthenospheric material beneath southwestern Anatolia. The hot asthenospheric material might have modified the structure of the crust via thermal erosion. The volcanic centers such as the Kirka-Afyon-Isparta (KAIVF) and Kula Volcanic Fields (KVF) and the high geothermal gradients in southwestern Anatolia are surface manifestations of the hot upwelling asthenosphere. The average heat flow values in southwestern Anatolia based on silica geothermometry and conventional temperature measurements are 107 ± 45 mW/m^2 and 97 ± 27 mW/m^2, respectively (Ilkişik et al., 1995). The highest heat flow value (>100 m/Wm^2) has been observed in the northeastern part of Gediz Graben near the Kula active volcanic center (Erkan et al., 2014). The volcanism in southwestern Anatolia is associated with rapid upwelling asthenosphere (Gülen et al., 1990; Tokçaer et al., 2005; Prelević et al., 2012). Moreover, the geochemical model for southwestern Anatolia, as constrained by trace element concentrations and the neodymium (Nd), strontium (Sr) & lead (Pb) isotopes, shows that the Kula volcanic rocks are formed by partial melting of asthenospheric mantle (Chakrabarti et al., 2011).

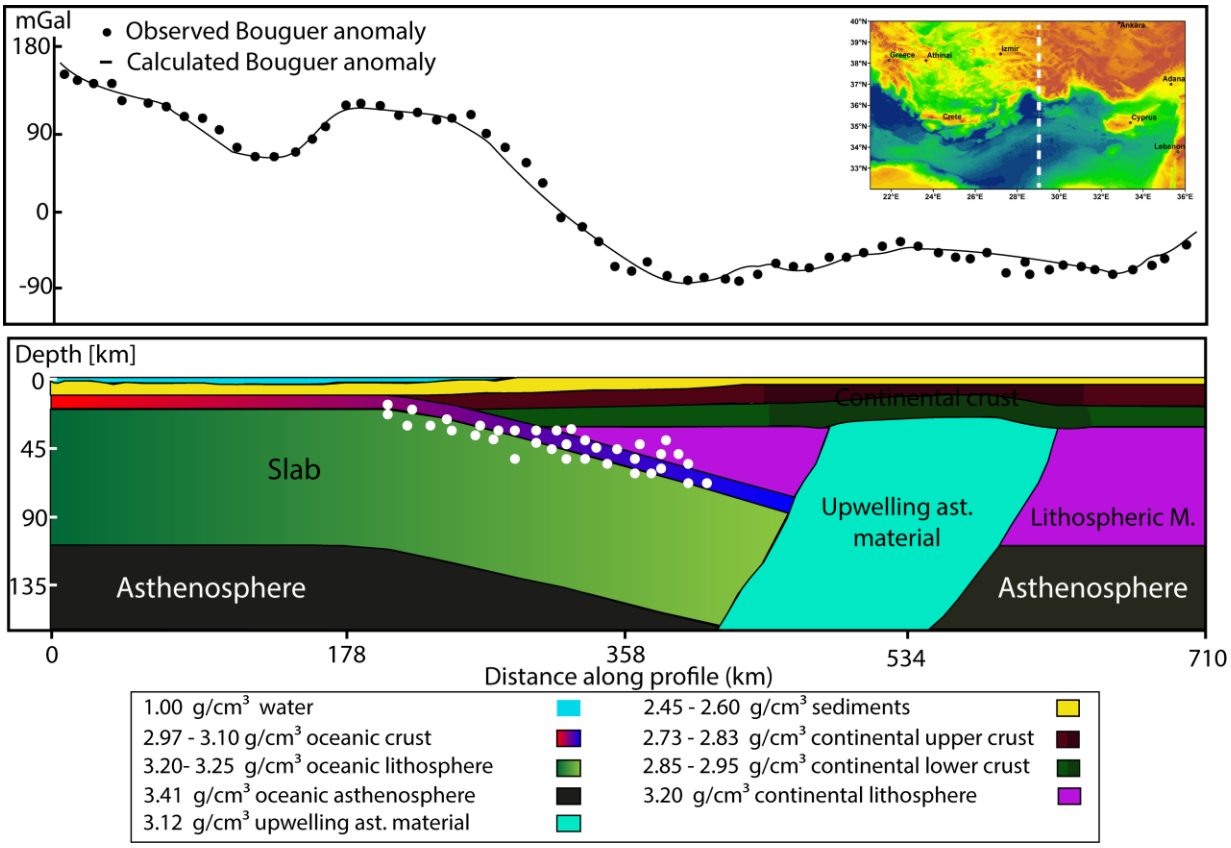

Figures 20. A 2.5-D gravity model of the southwestern Anatolian region at 29°E. The location of the profile is shown in Figures 1. The white circles are earthquake hypocenters.

7.2.4 Structure of the Cyprus Arc

Figure 21 shows the subduction of the African slab west of Cyprus at 31°E. This model depicts the crust and upper mantle structure of the western edge of the Cyprus slab. As in the other profiles, this model consists of water, sediment, upper-crust, lower-crust, the Hellenic slab (oceanic lithosphere), continental lithosphere and the asthenosphere. The model is 710 km long and extends from 34°N to 40°N. The depth to the bottom of the model is 165 km. The Bouguer gravity anomaly along this profile varies from -95 mGal to 126.

The dip of the Cyprus slab, as determined from gravity modeling and constrained by earthquake hypocenters, is ~ 60°. This is good agreement with the sub-vertical Cyprus slab

determined by Biryol et al., (2011). However, Salaün et al., (2012) interprets gentle dip based on seismic tomography.

The Moho depth in the overriding plate decreases from south to north (40 to 36 km). This change corresponds on the surface with tectonic transition from the Anatolide-Tauride to Sakarya zones. The crust along this profile is thicker than the asthenospheric window area, indicating that the effect of the low-velocity zone on the crustal structure of western Cyprus is minimal.

Sediment thickness along this profile decreases from south to north (4 – 12 km). This is consistent with previous sediment thickness determination (~4 -12 km in the Levantine and Herodotus Basins (Figure 1; Makris et al., 1983; Ginzburg et al., 1987; de Voogd et al., 1992; Ben-Avraham et al., 2002; Ergün et al., 2005; Makris et al., 2013).

As shown in Figure 22, the dip of the Cyprus slab at 33°E changes from sub-vertical to ~40^{o}. This is in agreement with the slab imaged by Salaün et al., (2012), but steeper than the slab modeled by Biryol et al., (2011). Both slab models are based on seismic tomography with different resolution. The position of the slab is constrained by earthquake hypocenters (Figure 22).

The average crustal thickness along this profile is ~42 km. There is a general tendency that the crust thickens from west to east (i.e. from the Aegean to the Anatolian regions). Previous studies showed that the Moho depth increases from west to east (Saunders et al., 1998; Angus et al., 2006; Zhu et al., 2006; Di Luccio and Pasyanos, 2007; Arslan et al., 2010; Çakır and Erduran, 2011; Mutlu and Karabulut, 2011; Ates et al., 2012; Karabulut et al., 2013; Tezel et al., 2007, 2010, 2013; Vanacore et al., 2013; Sayil et al., 2014; Kind et al., 2015).

The sediment thickness along this profile varies from 3 to 14 km and is consistent with previous work (Zhu et al., 2006; Akyol et al., 2006; Di Luccio et al., 2007; Işık et al., 2009; Tezel et al., 2013; Sayil et al., 2014).

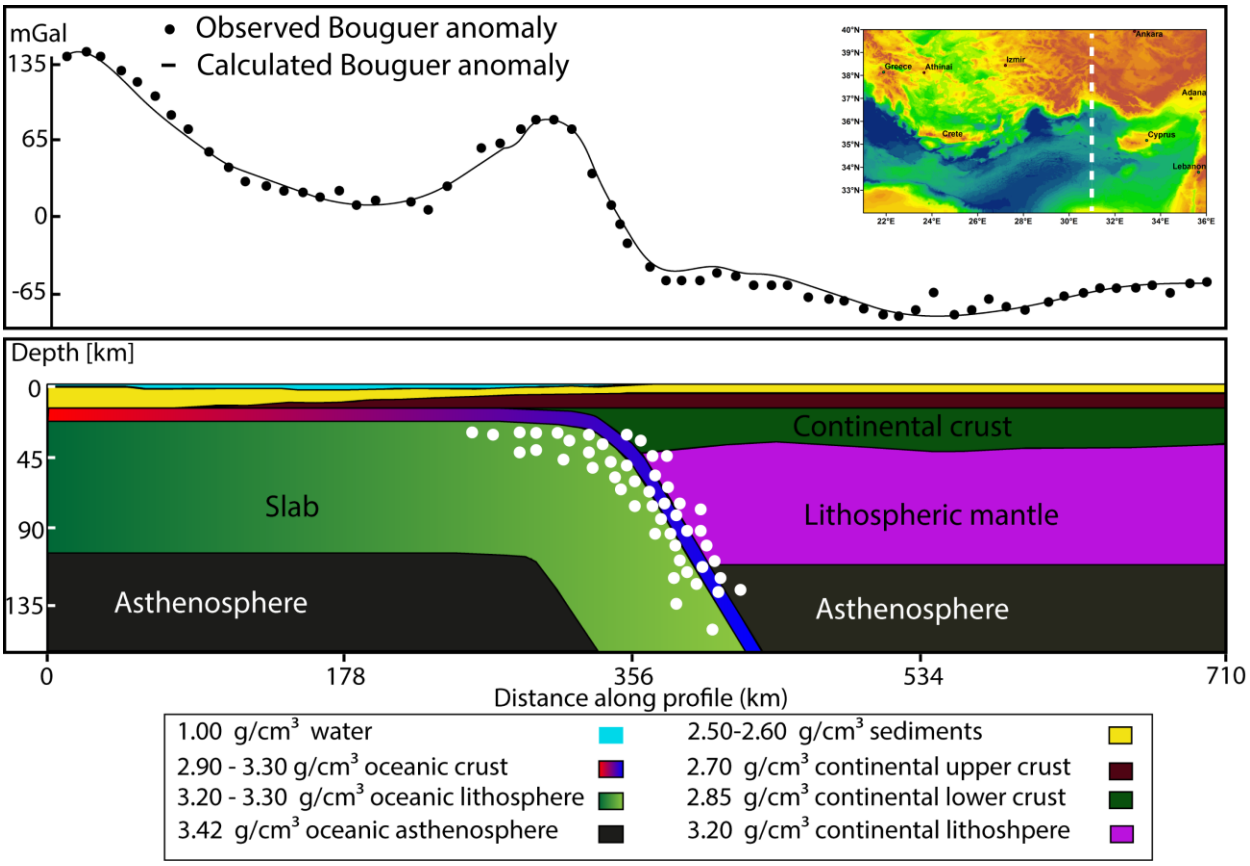

Figures 21. A 2.5-D gravity model of Cyprus at 31°E. The location of the profile is shown in Figure 1. The white circles are earthquake hypocenters.

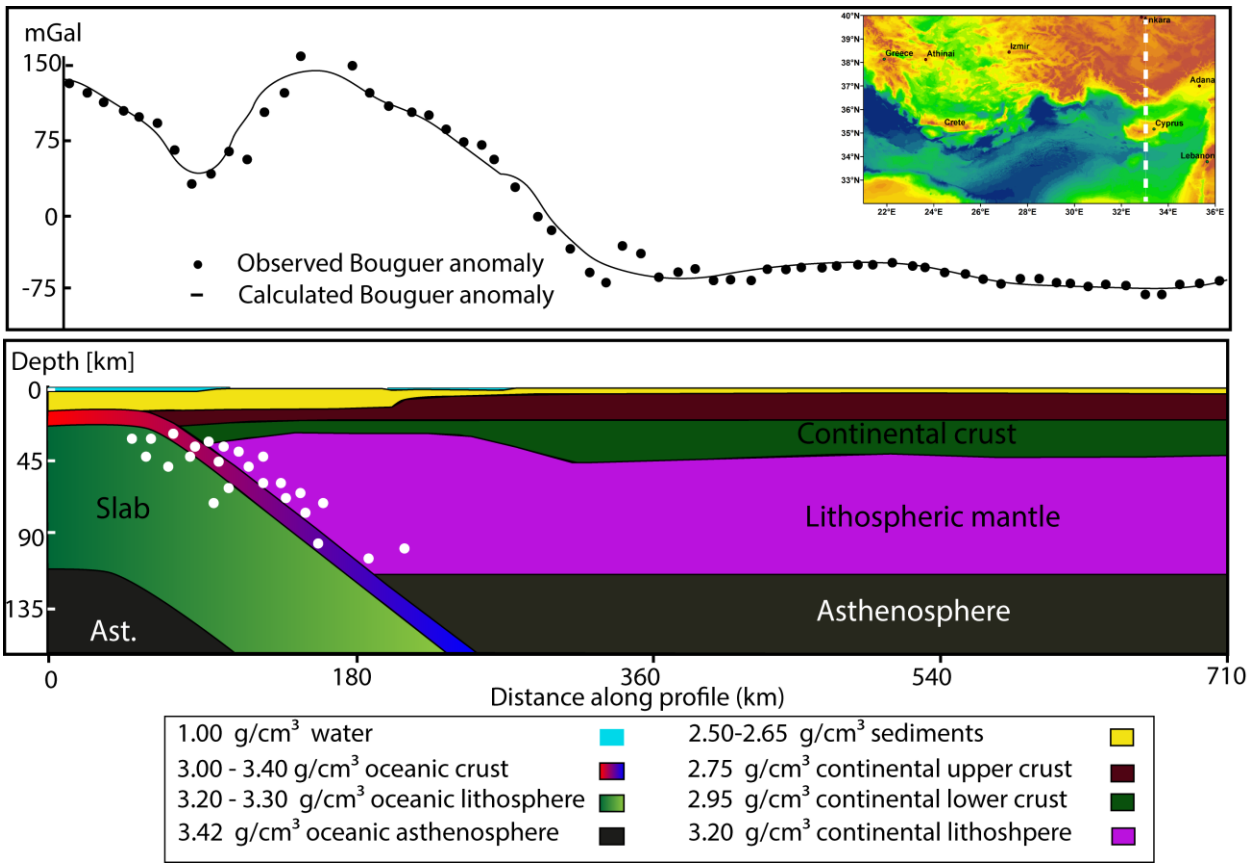

Figures 22. A 2.5-D gravity model of Cyprus arc at 33°E. The location of the profile is shown in Figure 1. The white circles are earthquake hypocenters.

7.2.5 3-D structure of the Aegean -Anatolian region

2.5-D gravity modeling is a first order approximation to a 3-D representation of the crust and upper mantle structure of the Earth. In order to determine the 3-D structure of the crust and upper mantle of the Aegean-Anatolian region, a 3-D gravity model has been developed (Figure 23). The geometries and densities of the 2.5-D models are used as inputs to GM-SYS-3D to create a 3-D representation of the crust and upper mantle structure of the study area. The model parameters were adjusted to fit the observed gravity field in a 3-D environment.

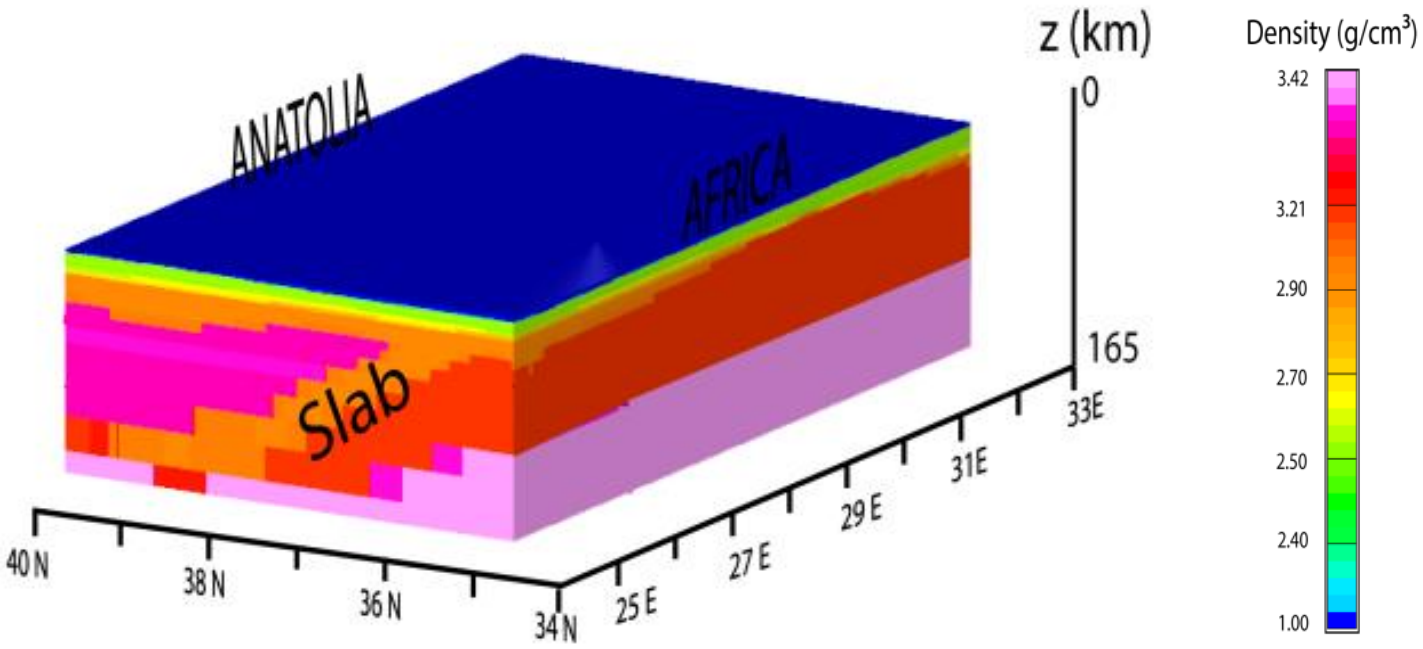

Figure 23. 3-D gravity model of the Aegean-Anatolian region. The model shows (from top to bottom) water, sediment, the crust, lithospheric mantle, the African slab and the asthenosphere.

The observed gravity data are well explained in terms of a low density asthenospheric material beneath southwestern Anatolia and slabs in the Hellenic & Cyprus subduction zones. The 3-D gravity model shows a thin crust beneath southwestern Anatolia between 28°E and 29.5°E. This is the region, where the African slab exhibits major slab-tear between the Hellenic and Cyprus trenches. The crustal thinning is attributed to a low-velocity zone (asthenospheric material) in the upper mantle. The same result was also obtained using 2.5-D gravity modeling. However, 3-D gravity modeling allows us to determine the ~280 km (Figure 25) the east-west dimension of the asthenospheric material. This is in good agreement with results of seismic tomography (~300 km; Spakman et al., 1993; Piromallo and Morelli 2003; Chang et al., 2010; Biryol et al., 2011; Salaün et al., 2012). Moreover, the 3-D model shows that

the dip of the subducting African plate varies with depth (Figure 24). This may imply that the style of subduction and rate of convergence of the African slab along the Hellenic and Cyprus trenches might have been variable.

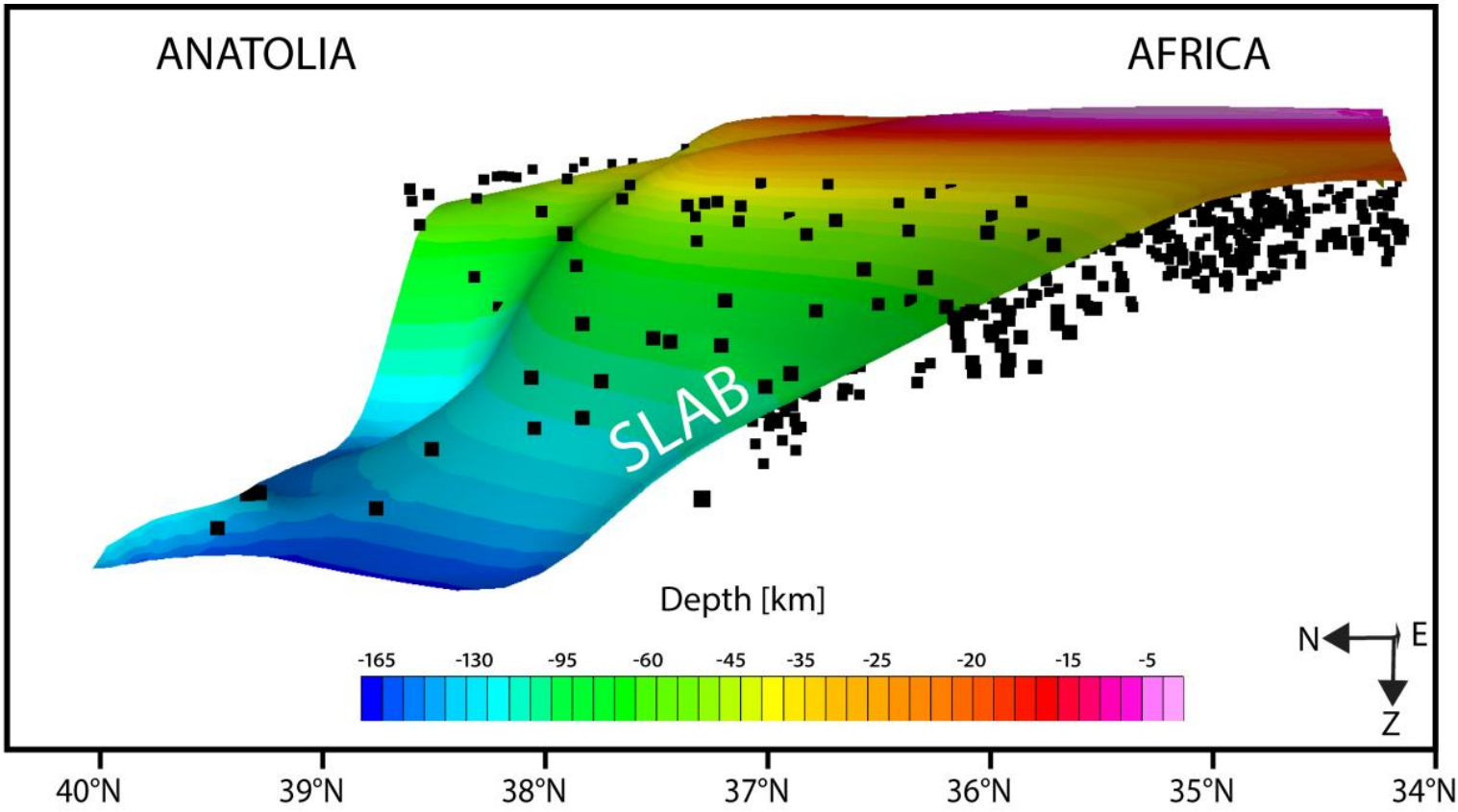

Figure 24. Depth to the top of the subducting African slab beneath the Aegean-Anatolian region derived from 3-D gravity modeling. Black squares are earthquake hypocenters. The earthquake events are from 1985 to 2015 (source: Boğaziçi University KOERI NEMCEQ/http://udim.koeri.boun.edu.tr/zeqdb/indexeng.asp)

8. DISCUSSIONS

The Aegean and southwestern Anatolia are classified as arc–back-arc regions dominated by slab roll-back (van Hinsbergen et al., 2005, 2010; Jolivet & Brun, 2010) and extensive post-Miocene extension that took place after the regions had experienced thickening of lithosphere during a series of collisional events of the Alpine orogeny from the late Cretaceous to the early Tertiary (Şengör et al., 1985; Yilmaz et al., 2000; Rimmele´ et al., 2003; Ring et al., 2003; Işık et al., 2004; Çemen et al., 2006; Westaway, 2006; Glodny & Hetzel, 2007).

Many authors suggest that slab tears, slab break off, and lithospheric delamination have played a major role in the evolution of the Anatolian plate as the African and Arabian plates collide with the Eurasian margin (Keskin et al., 2003; Şengör et al., 2003; Faccenna et al., 2006; Dilek & Altunkaynak 2009; Gans et al., 2009; Biryol et al., 2011; Cosentino et al., 2012; Salaün et al., 2012; Jolivet et al., 2013; Kind et al., 2015; Delph et al., 2015).

The existence of low-velocity zone beneath southwestern Anatolia, and hence slab-tear in the subducting African plate has been reported in many seismic tomography studies (de Boorder et al., 1998; Govers and Wortel, 2005; van Hinsbergen et al., 2010; Biryol et al., 2011; Salaün et al., 2012; Jolivet et al., 2013). The tear separates the subducting African plate into Hellenic and Cyprus slabs (Dilek and Sandvol, 2009; van Hinsbergen et al., 2010; Biryol et al., 2011; Mutlu and Karabulut, 2011; Salaün et al., 2012). The surface projection of the slab-tear (asthenospheric

window) coincides with the southwestern coast of Turkey and the Antalya Bay (Figure 3). The central section of the asthenospheric window underlies the Menderes Massif Complex.

The uppermost mantle, including the low-velocity zone, is well resolved by seismic tomography. However, the crystalline basement and the lower crust are not well resolved due to limited resolution of the seismic tomography (~ 50 km; Biryol et al., 2011).

In this study it is hypothesized that the hot asthenospheric material may have affected the crustal structure in southwestern Anatolia. The hypothesis is tested using 2.5-D and 3-D modeling of gravity data. The spatial resolution of the gravity data is ~10 km. The gravity model revealed a low-velocity zone in the upper mantle beneath southwestern Anatolia. The crust in southwestern Anatolia, as determined from gravity modeling, is significantly thin (24 – 30 km; e.g. Menderes Massif Complex; Figure 25). The thinning above the asthenospheric window area may be partly caused by thermal erosion attributed to the hot asthenospheric material in the upper mantle and extensional tectonics related to the southwest retreating Hellenic trench. The magmatic centers and high heat flow in the Menderes Massif Complex are surface manifestations of the asthenospheric flow beneath southwestern Anatolia.

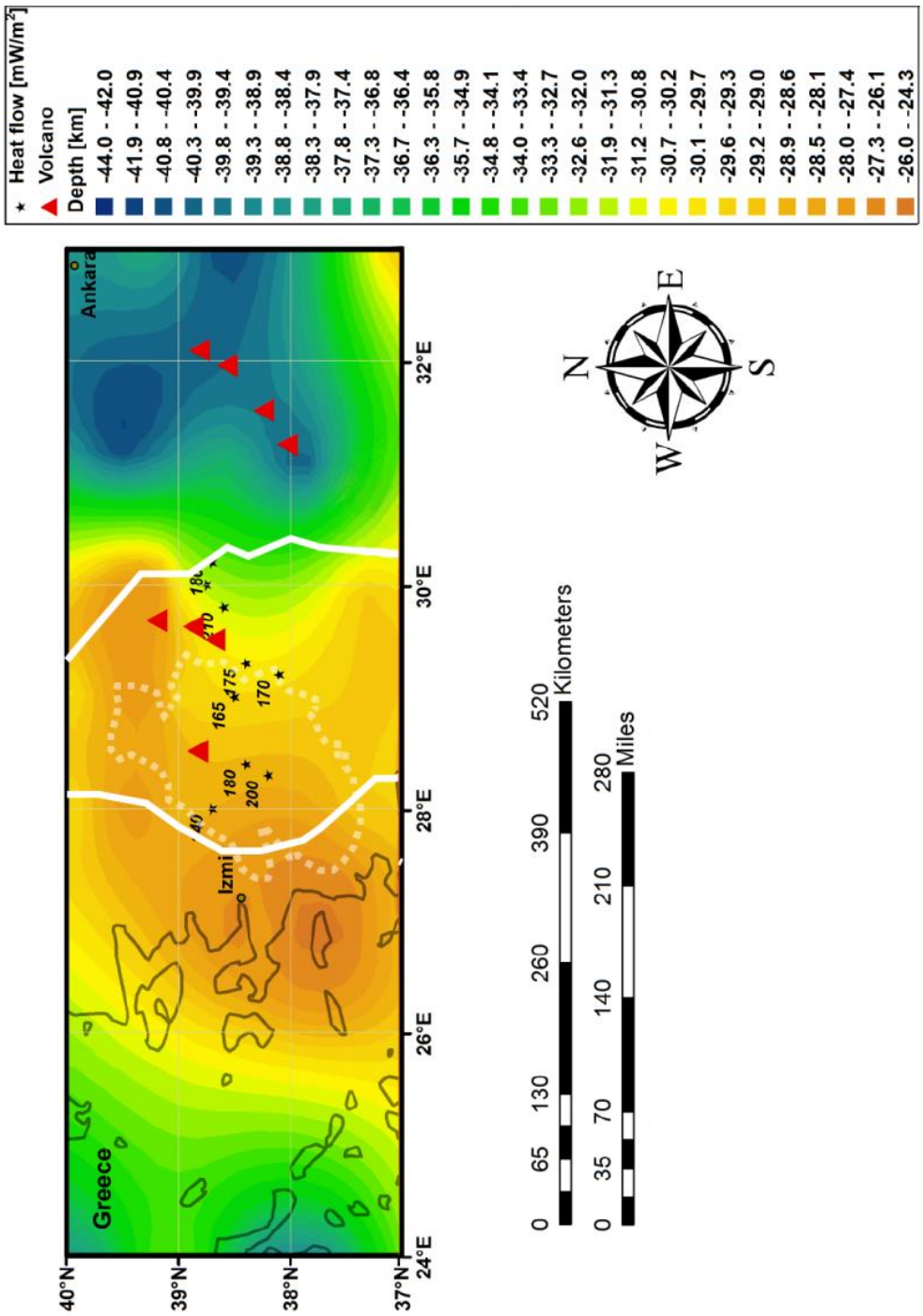

Figure 25. Moho depth map of the Aegean-Anatolian region from 3-D gravity data modeling. White dashed line shows the Menderes Massif Complex. Solid white line shows the location of the slow velocity anomaly imaged by seismic tomography (Biryol et al., 2011). Red triangles are for volcanoes. Black small stars are heat flow from Akin et al., (2014).

9. CONCLUSIONS

The effect of a low-velocity zone on crustal structure in southwestern Anatolia and the Aegean has been assessed using satellite and terrestrial gravity data modeling. The gravity model is constrained by receiver function analysis and seismic tomography. The gravity model reveals the presence of hot asthenospheric material (asthenospheric window) beneath Southwestern Anatolia. The crust above the asthenospheric window, where the subducted African slab exhibits major lateral tears, is relatively thin. The crustal thickness within the asthenospheric window area varies from 24 to 29 km. In contrast, the regions outside the asthenospheric window area exhibit by far the largest crustal thickness (30 – 42 km). The observed crustal thinning in the asthenospheric window area might be attributed to thermal erosion induced by an upwelling hot asthenospheric material and extensional tectonics related to the southwest retreating Hellenic trench and westward movement of the Anatolian microplate. Thus, compressional and extensional tectonic regions can undergo changes in structure and composition in response to extensional tectonics as well as thermal erosion associated with asthenospheric flow in the upper mantle.

The inverse correlation of the broad regional gravity low and topography indicates the presence of compensating masses beneath the Hellenides and Anatolian plateau. The high topography in Southwestern Anatolia also coincides with the location of the low-velocity zone in the upper mantle. The inverse correlation of high topography with low-gravity & low-velocity suggests that the southwestern Anatolian region is dynamically supported by convective

processes in the upper mantle. The high elevation of deformed areas in Anatolia is attributed to the convective cell in the upper mantle (Faccenna et al., 2014).

REFERENCES

Akiman, O., Erler, A., Göncüoğlu, M. C., Güleç, N., Geven, A., Türeli, T. K., & Kadioğlu, Y. K. (1993). Geochemical characteristics of granitoids along the western margin of the Central Anatolian Crystalline Complex and their tectonic implications. *Geological Journal*, *28*(3-4), 371-382.

Akin, U., Ulugergerli, E. U., & Kutlu, S. (2014). The assessment of geothermal potential of turkey by means of heat flow estimation. *Bulletin Of The Mineral Research and Exploration*, *149*(149).

Akyol, N., Zhu, L., Mitchell, B. J., Sözbilir, H., & Kekovalı, K. (2006). Crustal structure and local seismicity in western Anatolia. *Geophysical Journal International*, *166*(3), 1259-1269.

Al-Lazki, A. I., Sandvol, E., Seber, D., Barazangi, M., Turkelli, N., & Mohamad, R. (2004). Pn tomographic imaging of mantle lid velocity and anisotropy at the junction of the Arabian, Eurasian and African plates. *Geophysical Journal International*, *158*(3), 1024-1040.

Altunkaynak, Ş., & Dilek, Y. (2006). Timing and nature of postcollisional volcanism in western Anatolia and geodynamic implications. *Geological Society of America Special Papers*, *409*, 321-351.

Amante, C., & Eakins, B. W. (2009). *ETOPO1 1 arc-minute global relief model: procedures, data sources and analysis* (p. 19). US Department of Commerce, National Oceanic and Atmospheric Administration, National Environmental Satellite, Data, and Information Service, National Geophysical Data Center, Marine Geology and Geophysics Division.

Amaru, M. L. (2007). Global travel time tomography with 3-D reference models. *Geologica Ultraiectina*, *274*.

Andersen, O. B., and P. Knudsen (1998), Global marine gravity field fromthe ERS-1 and GEOSAT geodetic mission altimetry, J. Geophys. Res., 103, 8129–8137.

Angus, D. A., Wilson, D. C., Sandvol, E., & Ni, J. F. (2006). Lithospheric structure of the Arabian and Eurasian collision zone in eastern Turkey from S-wave receiver functions. *Geophysical Journal International*, *166*(3), 1335-1346.

Armijo, R., Meyer, B., Hubert, A., & Barka, A. (1999). Westward propagation of the North Anatolian fault into the northern Aegean: Timing and kinematics. *Geology*, *27*(3), 267-270.

Arslan, S., Akin, U., & Alaca, A. (2010). Investigation of crustal structure of Turkey by means of gravity data. *Mineral Research Exploration Bulletin*, *140*, 55-71.

Ates, A., Bilim, F., Buyuksarac, A., Aydemir, A., Bektas, O., & Aslan, Y. (2012). Crustal structure of Turkey from aeromagnetic, gravity and deep seismic reflection data. *Surveys in geophysics*, *33*(5), 869-885.

Aydan, Ö., & Kumsar, H. (2014). Assessment of the earthquake potential of the west Aegean region of Turkey based on seismicity, tectonics, crustal deformation and geo-archaeological evidence and its geotechnical aspects. *Bulletin of Engineering Geology and the Environment*, 1-19.

Bakırcı, T., Yoshizawa, K., & Özer, M. F. (2012). Three-dimensional S-wave structure of the upper mantle beneath Turkey from surface wave tomography. *Geophysical Journal International*, *190*(2), 1058-1076.

Barka, A. A. (1992). The north Anatolian fault zone. In *Annales tectonicae* (Vol. 6, No. Suppl, pp. 164-195).

Ben-Avraham, Z., Ginzburg, A., Makris, J., & Eppelbaum, L. (2002). Crustal structure of the Levant Basin, eastern Mediterranean. *Tectonophysics*, *346*(1), 23-43.

Bijwaard, H., Spakman, W., & Engdahl, E. R. (1998). Closing the gap between regional and global travel time tomography. *Journal of Geophysical Research: Solid Earth (1978–2012)*, *103*(B12), 30055-30078.

Bilim, F. (2007). Investigations into the tectonic lineaments and thermal structure of Kutahya–Denizli region, western Anatolia, from using aeromagnetic, gravity and seismological data. *Physics of the Earth and Planetary Interiors*, *165*(3), 135-146.

Bilim, F. (2011). Investigation of the Galatian volcanic complex in the northern central Turkey using potential field data. *Physics of the Earth and Planetary Interiors*, *185*(1), 36-43.

Biryol, C. B., Beck, S. L., Zandt, G., & Özacar, A. A. (2011). Segmented African lithosphere beneath the Anatolian region inferred from teleseismic P-wave tomography. *Geophysical Journal International*, *184*(3), 1037-1057.

Blakely, R. J. (1996). *Potential theory in gravity and magnetic applications*. Cambridge University Press, 441 pages.

Bohnhoff, M., Makris, J., Papanikolaou, D., & Stavrakakis, G. (2001). Crustal investigation of the Hellenic subduction zone using wide aperture seismic data. *Tectonophysics*, *343*(3), 239-262.

Burger, H. R. (1992). Burger, H. R., & Burger, D. C. (1992). *Exploration geophysics of the shallow subsurface*. Englewood Cliffs, N.J: Prentice Hall.

Çakır, Ö., Erduran, M., Çınar, H., & Yılmaztürk, A. (2000). Forward modelling receiver functions for crustal structure beneath station TBZ (Trabzon, Turkey). *Geophysical Journal International*, *140*(2), 341-356.

Çakır, Ö., & Erduran, M. (2004). Constraining crustal and uppermost mantle structure beneath station TBZ (Trabzon, Turkey) by receiver function and dispersion analyses. *Geophysical Journal International*, *158*(3), 955-971.

Çakır, Ö., & Erduran, M. (2011). On the P and S receiver functions used for inverting the one-dimensional upper mantle shear-wave velocities. *Surveys in geophysics*, *32*(1), 71-98.

Cambaz, M. D., & Karabulut, H. (2010). Love-wave group velocity maps of Turkey and surrounding regions. *Geophysical Journal International*, *181*(1), 502-520.

Casten, U., & Snopek, K. (2006). Gravity modelling of the Hellenic subduction zone—a regional study. *Tectonophysics*, *417*(3), 183-200.

Catlos, E. J., & Çemen, I. (2005). Monazite ages and the evolution of the Menderes Massif, western Turkey. *International Journal of Earth Sciences*, *94*(2), 204-217.

Çemen, I., Göncüoglu, M. C., & Dirik, K. (1999). Structural evolution of the Tuzgölü basin in Central Anatolia, Turkey. *The Journal of geology*, *107*(6), 693-706.

Çemen, I., Catlos, E. J., Göğüs, O., & Özerdem, C. (2006). Postcollisional extensional tectonics and exhumation of the Menderes massif in the Western Anatolia extended terrane, Turkey. *Geological Society of America Special Papers*, *409*, 353-379.

Çemen, I., Helvaci, C., & Ersoy, E. Y. (2014). Cenozoic extensional tectonics in western and central Anatolia, Turkey: Introduction. *Tectonophysics*, *635*, 1-5.

Chakrabarti, R., Basu, A. R., & Ghatak, A. (2011). Chemical geodynamics of western Anatolia. *International Geology Review*, *54*(2), 227-248.

Chang, S. J., van der Lee, S., Flanagan, M. P., Bedle, H., Marone, F., Matzel, E. M., & Schmid, C. (2010). Joint inversion for three-dimensional S velocity mantle structure along the Tethyan margin. *Journal of Geophysical Research: Solid Earth (1978–2012)*, *115*(B8).

Chen, F., Siebel, W., Satir, M., Terzioğlu, M., & Saka, K. (2002). Geochronology of the Karadere basement (NW Turkey) and implications for the geological evolution of the Istanbul zone. *International Journal of Earth Sciences*, *91*(3), 469-481.

Christensen, N., & Mooney, W. (1995). Seismic velocity structure and composition of the continental crust: A global view. *Journal of Geophysical Research Atmospheres*, (100), 9761-9788.

Christova, C., & Nikolova, S. B. (1993). The Aegean region: deep structures and seismological properties. *Geophysical Journal International*, *115*(3), 635-653.

Çifçi, G., Pamukçu, O., Çoruh, C., Çopur, S., & Sözbilir, H. (2011). Shallow and deep structure of a supradetachment basin based on geological, conventional deep seismic reflection sections and gravity data in the Buyuk Menderes Graben, western Anatolia. *Surveys in Geophysics*, *32*(3), 271-290.

Çoban, H., & Flower, M. F. (2007). Late Pliocene lamproites from Bucak, Isparta (southwestern Turkey): implications for mantle 'wedge'evolution during Africa-Anatolian plate convergence. *Journal of Asian Earth Sciences*, *29*(1), 160-176.

Cocard, M., Kahle, H. G., Peter, Y., Geiger, A., Veis, G., Felekis, S.,& Billiris, H. (1999). New constraints on the rapid crustal motion of the Aegean region: recent results inferred from GPS measurements (1993–1998) across the West Hellenic Arc, Greece. *Earth and Planetary Science Letters*, *172*(1), 39-47.

Cosentino, D., Schildgen, T. F., Cipollari, P., Faranda, C., Gliozzi, E., Hudáčková, N.,& Strecker, M. R. (2012). Late Miocene surface uplift of the southern margin of the Central Anatolian Plateau, Central Taurides, Turkey. *Geological Society of America Bulletin*, *124*(1-2), 133-145.

De Boorder, H., Spakman, W., White, S. H., & Wortel, M. J. R. (1998). Late Cenozoic mineralization, orogenic collapse and slab detachment in the European Alpine Belt. *Earth and Planetary Science Letters*, *164*(3), 569-575.

De Voogd, B., Truffert, C., Chamot-Rooke, N., Huchon, P., Lallemant, S., & Le Pichon, X. (1992). Two-ship deep seismic soundings in the basins of the Eastern Mediterranean Sea (Pasiphae cruise). *Geophysical Journal International*, *109*(3), 536-552.

Delaloye, M., & Bingol, E. (2000). Granitoids from western and northwestern Anatolia: geochemistry and modeling of geodynamic evolution. *International Geology Review*, *42*(3), 241-268.

Delph, J. R., Biryol, C. B., Beck, S. L., Zandt, G., & Ward, K. M. (2015). Shear wave velocity structure of the Anatolian Plate: anomalously slow crust in southwestern Turkey. *Geophysical Journal International*, *202*(1), 261-276.

Dewey, J. F., & Şengör, A. C. (1979). Aegean and surrounding regions: complex multiplate and continuum tectonics in a convergent zone. *Geological Society of America Bulletin*, *90*(1), 84-92.

Di Luccio, F., & Pasyanos, M. E. (2007). Crustal and upper-mantle structure in the Eastern Mediterranean from the analysis of surface wave dispersion curves. *Geophysical Journal International*, *169*(3), 1139-1152.

Dilek, Y., & Altunkaynak, Ş. (2009). Geochemical and temporal evolution of Cenozoic magmatism in western Turkey: mantle response to collision, slab break-off, and lithospheric tearing in an orogenic belt. *Geological Society, London, Special Publications*, *311*(1), 213-233.

Dilek, Y., & Sandvol, E. (2009). Seismic structure, crustal architecture and tectonic evolution of the Anatolian-African Plate Boundary and the Cenozoic Orogenic Belts in the Eastern Mediterranean Region. *Geological Society, London, Special Publications*, *327*(1), 127-160.

Elitok, Ö., & Dolmaz, M. N. (2008). Mantle flow-induced crustal thinning in the area between the easternmost part of the Anatolian plate and the Arabian Foreland (E Turkey) deduced from the geological and geophysical data. *Gondwana Research*, *13*(3), 302-318.

Endrun, B., Ceranna, L., Meier, T., Bohnhoff, M., & Harjes, H. P. (2005). Modeling the influence of Moho topography on receiver functions: A case study from the central Hellenic subduction zone. *Geophysical research letters*,*32*(12).

Erduran, M., Çakır, Ö., Tezel, T., Şahin, Ş., & Alptekin, Ö. (2007). Anatolian surface wave evaluated at GEOFON station ISP Isparta, Turkey. *Tectonophysics*, *434*(1), 39-54.

Erduran, M., Endrun, B., & Meier, T. (2008). Continental vs. oceanic lithosphere beneath the eastern Mediterranean Sea—implications from Rayleigh wave dispersion measurements. *Tectonophysics*, *457*(1), 42-52.

Erduran, M. (2009). Teleseismic inversion of crustal S-wave velocities beneath the Isparta Station. *Journal of Geodynamics*, *47*(5), 225-236.

Ergün, M., Okay, S., Sari, C., Oral, E. Z., Ash, M., Hall, J., & Miller, H. (2005). Gravity anomalies of the Cyprus Arc and their tectonic implications. *Marine Geology*, *221*(1), 349-358.

Erkan, K. (2014). Crustal heat flow measurements in western Anatolia from borehole equilibrium temperatures. *Solid Earth Discussions*, *6*(1), 403-426.

Ersan, A., & Erduran, M. (2010). Orta Anadolu'nun kabuksal hız yapısının araştırılması. *Dicle Üniversitesi Mühendislik Fakültesi Mühendislik Dergisi*, *1*(1), 49-60 (in Turkish).

Faccenna, C., Bellier, O., Martinod, J., Piromallo, C., & Regard, V. (2006). Slab detachment beneath eastern Anatolia: A possible cause for the formation of the North Anatolian fault. *Earth and Planetary Science Letters*, *242*(1), 85-97.

Faccenna, C., Becker, T. W., Auer, L., Billi, A., Boschi, L., Brun, J. P. & Serpelloni, E. (2014). Mantle dynamics in the Mediterranean. *Reviews of Geophysics*, *52*(3), 283-332.

Fichtner, A., Saygin, E., Taymaz, T., Cupillard, P., Capdeville, Y., & Trampert, J. (2013). The deep structure of the North Anatolian fault zone. *Earth and Planetary Science Letters*, *373*, 109-117.

Förste, C., Bruinsma, S. L., Flechtner, F., Marty, J., Lemoine, J. M., Dahle, C., & Balmino, G. (2012, December). A preliminary update of the Direct approach GOCE Processing and a new release of EIGEN-6C. In *AGU Fall Meeting Abstracts* (Vol. 1, p. 0923).

Fytikas, M. D. (1980). Geothermal exploitation in Greece. In *Advances in European Geothermal Research* (pp. 213-237). Springer Netherlands.

Gans, C. R., Beck, S. L., Zandt, G., Biryol, C. B., & Özacar, A. A. (2009). Detecting the limit of slab break-off in central Turkey: new high-resolution Pn tomography results. *Geophysical Journal International*, *179*(3), 1566-1572.

Gardner, G. H. F., Gardner, L. W., & Gregory, A. R. (1974). Formation velocity and density-the diagnostic basics for stratigraphic traps. *Geophysics*, *39*(6), 770-780.

Gautier, P., Brun, J. P., Moriceau, R., Sokoutis, D., Martinod, J., & Jolivet, L. (1999). Timing, kinematics and cause of Aegean extension: a scenario based on a comparison with simple analogue experiments. *Tectonophysics*, *315*(1), 31-72.

Gesret, A., Laigle, M., Diaz, J., Sachpazi, M., Charalampakis, M., & Hirn, A. (2011). Slab top dips resolved by teleseismic converted waves in the Hellenic subduction zone. *Geophysical Research Letters*, *38*(20).

Gessner, K., Gallardo, L. A., Markwitz, V., Ring, U., & Thomson, S. N. (2013). What caused the denudation of the Menderes Massif: Review of crustal evolution, lithosphere structure, and dynamic topography in southwest Turkey. *Gondwana research*, *24*(1), 243-274.

Ginzburg, A., & Ben-Avraham, Z. (1987). The deep structure of the central and southern Levant continental margin. *Ann. Tectonicae*, *1*(2), 105-115.

Glodny, J., & Hetzel, R. (2007). Precise U–Pb ages of syn-extensional Miocene intrusions in the central Menderes Massif, western Turkey. *Geological Magazine*, *144*(02), 235-246.

Gorshkov, G. S. (1972). Progress and problems in volcanology. *Tectonophysics*, *13*(1), 123-140.

Govers, R., & Wortel, M. J. R. (2005). Lithosphere tearing at STEP faults: response to edges of subduction zones. *Earth and Planetary Science Letters*, *236*(1), 505-523.

Gülen, L. (1990). Isotopic characterization of Aegean magmatism and geodynamic evolution of the Aegean subduction. In *International Earth Science Colloquium on the Aegean Region (IESCA), Izmir, Turkey: Proceedings* (Vol. 2, pp. 143-166).

Gürer, A., Pinçe, A., Gürer, Ö. F., & Ilkişik, O. M. (2002). Resistivity distribution in the Gediz Graben and its implications for crustal structure. *Turkish Journal of Earth Sciences*, *11*(1), 15-25.

Harrison, R. W., Newell, W. L., Batıhanlı, H., Panayides, I., McGeehin, J. P., Mahan, S.& Necdet, M. (2004). Tectonic framework and Late Cenozoic tectonic history of the northern part of Cyprus: implications for earthquake hazards and regional tectonics. *Journal of Asian Earth Sciences*, *23*(2), 191-210.

Hatzfeld, D., & Martin, C. (1992). The Aegean intermediate seismicity defined by ISC data. *Earth Planet. Sci. Lett*, *113*, 267-275.

Hetzel, R., & Reischmann, T. (1996). Intrusion age of Pan-African augen gneisses in the southern Menderes Massif and the age of cooling after Alpine ductile extensional deformation. *Geological Magazine*, *133*(05), 565-572.

Horasan, G., Gülen, L., Pinar, A., Kalafat, D., Özel, N., Kuleli, H. S., & Işikara, A. M. (2002). Lithospheric structure of the Marmara and Aegean regions, western Turkey. *Bulletin of the Seismological Society of America*, *92*(1), 322-329.

Hubbert, M. K. (1948). A line-integral method of computing the gravimetric effects of two-dimensional masses. *Geophysics*, *13*(2), 215-225.

Ilkişik, O. M. (1995). Regional heat flow in western Anatolia using silica temperature estimates from thermal springs. *Tectonophysics*, *244*(1), 175-184.

Imprescia, P., Pondrelli, S., Vannucci, G., & Gresta, S. (2012). Regional centroid moment tensor solutions in Cyprus from 1977 to the present and seismotectonic implications. *Journal of seismology*, *16*(2), 147-167.

Işık, V., Tekeli, O., & Seyitoglu, G. (2004). The 40 Ar/39 Ar age of extensional ductile deformation and granitoid intrusion in the northern Menderes core complex: implications for the initiation of extensional tectonics in western Turkey. *Journal of Asian Earth Sciences*, *23*(4), 555-566.

Işık, M., & Şenel, H. (2009). 3D gravity modeling of Büyük Menderes basin in Western Anatolia using parabolic density function. *Journal of Asian Earth Sciences*, *34*(3), 317-325.

Jackson, J. (1992). Partitioning of strike-slip and convergent motion between Eurasia and Arabia in eastern Turkey and the Caucasus. *Journal of Geophysical Research: Solid Earth (1978–2012)*, *97*(B9), 12471-12479.

Jackson, J. (1994). Active tectonics of the Aegean region. *Annual Review of Earth and Planetary Sciences*, *22*, 239-271.

Jolivet, L., & Faccenna, C. (2000). Mediterranean extension and the Africa-Eurasia collision. *Tectonics*, *19*(6), 1095-1106.

Jolivet, L., & Brun, J. P. (2010). Cenozoic geodynamic evolution of the Aegean. *International Journal of Earth Sciences*, *99*(1), 109-138.

Jolivet, L., Faccenna, C., Huet, B., Labrousse, L., Le Pourhiet, L., Lacombe, O. & Driussi, O. (2013). Aegean tectonics: Strain localisation, slab tearing and trench retreat. *Tectonophysics*, *597*, 1-33.

Kahle, H. G., Cocard, M., Peter, Y., Geiger, A., Reilinger, R., McClusky, S.,& Veis, G. (1999). The GPS strain rate field in the Aegean Sea and western Anatolia. *Geophysical research letters*, *26*(16), 2513-2516.

Kalyoncuoğlu, Ü. Y., Elitok, Ö., Dolmaz, M. N., & Anadolu, N. C. (2011). Geophysical and geological imprints of southern Neotethyan subduction between Cyprus and the Isparta Angle, SW Turkey. *Journal of Geodynamics*, *52*(1), 70-82.

Karabulut, H., Paul, A., Ergün, T. A., Hatzfeld, D., Childs, D. M., & Aktar, M. (2013). Long-wavelength undulations of the seismic Moho beneath the strongly stretched Western Anatolia. *Geophysical Journal International*, *194*(1), 450-464.

Karagianni, E. E., Panagiotopoulos, D. G., Panza, G. F., Suhadolc, P., Papazachos, C. B., Papazachos, B. C.,& Vuan, A. (2002). Rayleigh wave group velocity tomography in the Aegean area. *Tectonophysics*, *358*(1), 187-209.

Karagianni, E. E., Papazachos, C. B., Panagiotopoulos, D. G., Suhadolc, P., Vuan, A., & Panza, G. F. (2005). Shear velocity structure in the Aegean area obtained by inversion of Rayleigh waves. *Geophysical Journal International*, *160*(1), 127-143.

Keskin, M. (2003). Magma generation by slab steepening and breakoff beneath a subduction-accretion complex: An alternative model for collision-related volcanism in Eastern Anatolia, Turkey. *Geophysical Research Letters*, *30*(24).

Kind, R., Eken, T., Tilmann, F., Sodoudi, F., Taymaz, T., Bulut, F.& Schneider, F. (2015). Thickness of the lithosphere beneath Turkey and surroundings from S-receiver functions. *Solid Earth Discussions*, *7*, 1315-1346.

Knapmeyer, M. (1999). Geometry of the Aegean Benioff zones. *Annuals of Geophysics*, *42*(1).

Koulakov, I., Tychkov, S., Bushenkova, N., & Vasilevsky, A. (2002). Structure and dynamics of the upper mantle beneath the Alpine–Himalayan orogenic belt, from teleseismic tomography. *Tectonophysics*, *358*(1), 77-96.

Koulakov, I., & Sobolev, S. V. (2006). Moho depth and three-dimensional P and S structure of the crust and uppermost mantle in the Eastern Mediterranean and Middle East derived from tomographic inversion of local ISC data. *Geophysical Journal International*, *164*(1), 218-235.

Kustowski, B., Ekström, G., & Dziewoński, A. M. (2008). The shear-wave velocity structure in the upper mantle beneath Eurasia. *Geophysical Journal International*, *174*(3), 978-992.

Landès, M., Hubans, F., Shapiro, N. M., Paul, A., & Campillo, M. (2010). Origin of deep ocean microseisms by using teleseismic body waves. *Journal of Geophysical Research: Solid Earth (1978–2012)*, *115*(B5).

Langseth, M. G., & Taylor, P. T. (1967). Recent heat flow measurements in the Indian Ocean. *Journal of Geophysical Research*, *72*(24), 6249-6260.

Le Pichon, X., & Angelier, J. (1979). The Hellenic arc and trench system: a key to the neotectonic evolution of the eastern Mediterranean area. *Tectonophysics*, *60*(1), 1-42.

Le Pichon, X., & Angelier, J. (1981). The Aegean Sea: Philosophical Transaction of the Royal Society of London A, v. 300. *ndash*, *372*, 357.

Le Pichon, X., Chamot-Rooke, N., Lallemant, S., Noomen, R., & Veis, G. (1995). Geodetic determination of the kinematics of central Greece with respect to Europe: Implications for eastern Mediterranean tectonics. *J. geophys. Res*, *100*(12), 675-12.

Lee, W. H., & Uyeda, S. (1965). Review of heat flow data. In *Terrestrial heat flow* (Vol. 8, pp. 87-190). American Geophysical Union Washington, DC.

Levshin, A., Ratnikova, L., & Berger, J. (1992). Peculiarities of surface-wave propagation across central Eurasia. *Bulletin of the Seismological Society of America*, *82*(6), 2464-2493.

Levshin, A. L., Ritzwoller, M. H., & Ratnikova, L. I. (1994). The nature and cause of polarization anomalies of surface waves crossing northern and central Eurasia. *Geophysical Journal International*, *117*(3), 577-590.

Li, X., Bock, G., Vafidis, A., Kind, R., Harjes, H. P., Hanka, W. & Yuan, X. (2003). Receiver function study of the Hellenic subduction zone: imaging crustal thickness variations and the oceanic Moho of the descending African lithosphere. *Geophysical Journal International*, *155*(2), 733-748.

Ligdas, C. N., Main, I. G., & Adams, R. D. (1990). 3-D structure of the lithosphere in the Aegean region. *Geophysical Journal International*, *102*(1), 219-229.

Lips, A. L., Cassard, D., Sözbilir, H., Yilmaz, H., & Wijbrans, J. R. (2001). Multistage exhumation of the Menderes massif, western Anatolia (Turkey). *International Journal of Earth Sciences*, *89*(4), 781-792.

Ludwig, W. J., Nafe, J. E., & Drake, C. L. (1970). Seismic refraction. *The sea*, *4*(Part 1), 53-84.

Makris, J. (1978). The crust and upper mantle of the Aegean region from deep seismic soundings. *Tectonophysics*, *46*(3), 269-284.

Makris, J., Abraham, Z. B., Behle, A., Ginzburg, A., Giese, P., Steinmetz, L.,& Eleftheriou, S., (1983). Seismic refraction profiles between Cyprus and Israel and their interpretation. *Geophysical Journal International*, *75*(3), 575-591.

Makris, J., & Stobbe, C. (1984). Physical properties and state of the crust and upper mantle of the Eastern Mediterranean Sea deduced from geophysical data. *Marine Geology*, *55*(3), 347-363.

Makris, J., & Yegorova, T. (2006). A 3-D density–velocity model between the Cretan Sea and Libya. *Tectonophysics*, *417*(3), 201-220.

Makris, J., & Papoulia, J. (2009). Tectonic evolution of Zakinthos island from deep seismic soundings: thrusting and its association with the Triassic evaporates. In *Proceedings for the Intl. Symposium and Field trip Evaporites: Sedimentology, Evaluation and Economic Significance* (pp. 47-54).

Makris, J., 2010. Geophysical studies and tectonism of the Hellenides, *Bull. Geol. Soc. Greece,* XLIII(1), 32–45.

Makris, J., Papoulia, J., & Yegorova, T. (2013). A 3-D density model of Greece constrained by gravity and seismic data. *Geophysical Journal International*, ggt059.

Malehmir, A. (2007). 3D Geophysical and Geological Modeling in the Skellefte District: Implications for Targeting Ore Deposits.

Marone, F., Van Der Meijde, M., Van Der Lee, S., & Giardini, D. (2003). Joint inversion of local, regional and teleseismic data for crustal thickness in the Eurasia–Africa plate boundary region. *Geophysical Journal International*, *154*(2), 499-514.

Marquering, H., & Snieder, R. (1996). Shear-wave velocity structure beneath Europe, the northeastern Atlantic and western Asia from waveform inversions including surface-wave mode coupling. *Geophysical Journal International*, *127*(2), 283-304.

McClusky, S., Balassanian, S., Barka, A., Demir, C., Ergintav, S., Georgiev, I. & Veis, G. (2000). Global Positioning System constraints on plate kinematics and dynamics in the eastern

Mediterranean and Caucasus. *Journal of Geophysical Research: Solid Earth (1978–2012)*, *105*(B3), 5695-5719.

McClusky, S., Reilinger, R., Mahmoud, S., Sari, D. B., & Tealeb, A. (2003). GPS constraints on Africa (Nubia) and Arabia plate motions. *Geophysical Journal International*, *155*(1), 126-138.

McKenzie, D. (1967). Some remarks on heat flow and gravity anomalies.*Journal of Geophysical Research*, *72*(24), 6261-6273.

McKenzie, D. (1972). Active tectonics of the Mediterranean region. *Geophysical Journal International*, *30*(2), 109-185.

McKenzie, D. (1978). Active tectonics of the Alpine—Himalayan belt: the Aegean Sea and surrounding regions. *Geophysical Journal International*, *55*(1), 217-254.

Meier, T., Dietrich, K., Stöckhert, B., & Harjes, H. P. (2004). One-dimensional models of shear wave velocity for the eastern Mediterranean obtained from the inversion of Rayleigh wave phase velocities and tectonic implications. *Geophysical Journal International*, *156*(1), 45-58.

Meier, T., Becker, D., Endrun, B., Rische, M., Bohnhoff, M., Stöckhert, B., & Harjes, H. P. (2007). A model for the Hellenic subduction zone in the area of Crete based on seismological investigations. *Geological Society, London, Special Publications*, *291*(1), 183-199.
Mutlu, H., Güleç, N., & Hilton, D. R. (2008). Helium–carbon relationships in geothermal fluids of western Anatolia, Turkey. *Chemical Geology*, *247*(1), 305-321.

Meulenkamp, J. E., Wortel, M. J. R., Van Wamel, W. A., Spakman, W., & Strating, E. H. (1988). On the Hellenic subduction zone and the geodynamic evolution of Crete since the late Middle Miocene. *Tectonophysics*, *146*(1), 203-215.

Meulenkamp, J. E., Van der Zwaan, G. J., & Van Wamel, W. A. (1994). On Late Miocene to Recent vertical motions in the Cretan segment of the Hellenic arc. *Tectonophysics*, *234*(1), 53-72.

Mindevalli, O. Y., & Mitchell, B. J. (1989). Crustal structure and possible anisotropy in Turkey from seismic surface wave dispersion. *Geophysical Journal International*, *98*(1), 93-106.

Monod, O., Kozlu, H., Ghienne, J. F., Dean, W. T., Günay, Y., Hérissé, A. L.,& Robardet, M. (2003). Late Ordovician glaciation in southern Turkey. *Terra Nova*, *15*(4), 249-257.

Morelli, C. (1976). Modern standards for gravity surveys. *Geophysical Journal of the Royal Astronomical Society*, *45*(1), 199-199.

Mutlu, A. K., & Karabulut, H. (2011). Anisotropic Pn tomography of Turkey and adjacent regions. *Geophysical Journal International*, *187*(3), 1743-1758.

Nafe, J. E., & Drake, C. L. (1957). Variation with depth in shallow and deep water marine sediments of porosity, density and the velocities of compressional and shear waves. *Geophysics*, *22*(3), 523-552.

Necioğlu, A., Maddison, B., & Türkelli, N. (1981). A study of crustal and upper mantle structure of northwestern Turkey. *Geophysical Research Letters*, *8*(1), 33-35.

Nettleton, L. L. (1976). *Gravity and magnetics in oil prospecting*. McGraw-Hill Companies.

Netzeband, G. L., Gohl, K., Hübscher, C. P., Ben-Avraham, Z., Dehghani, G. A., Gajewski, D., & Liersch, P. (2006). The Levantine Basin—crustal structure and origin. *Tectonophysics*, *418*(3), 167-188.

Nikolintaga, I., V. Karakostas, E. Papadimitriou and F. Vallianatos (2007): Velocity models inferred from P-waves travel time curves in South Aegean, *Bull. Geol. Soc. Greece*, XXXX, 1187-1198.

Okay, A. I. (1984). Distribution and characteristics of the north-west Turkish blueschists. *Geological Society, London, Special Publications*, *17*(1), 455-466.

Okay, A.I., (1989). Geology of the Menderes Massif and the Lycian Nappes south of Denizli, western Taurides. *Mineral Research Exploration Bulletin 109*, 37–51.

Okay, A. I., Şengör, A. C., & Görür, N. (1994). Kinematic history of the opening of the Black Sea and its effect on the surrounding regions. *Geology*, *22*(3), 267-270.

Okay, A. I., & Tüysüz, O. (1999). Tethyan sutures of northern Turkey. *Geological Society, London, Special Publications*, *156*(1), 475-515.

Okay, A. I. (2002). Jadeite–chloritoid–glaucophane–lawsonite blueschists in north-west Turkey: unusually high P/T ratios in continental crust. *Journal of Metamorphic Geology*, *20*(8), 757-768.

Okay, A. I., Satir, M., & Siebel, W. (2006). Pre-Alpide Palaeozoic and Mesozoic orogenic events in the Eastern Mediterranean region. *Geological Society, London, Memoirs*, *32*(1), 389-405.

Özacar, A. A., Gilbert, H., & Zandt, G. (2008). Upper mantle discontinuity structure beneath East Anatolian Plateau (Turkey) from receiver functions. *Earth and Planetary Science Letters*, *269*(3), 427-435.

Özacar, A. A., Zandt, G., Gilbert, H., & Beck, S. L. (2010). Seismic images of crustal variations beneath the East Anatolian Plateau (Turkey) from teleseismic receiver functions. *Geological Society, London, Special Publications*, *340*(1), 485-496.

Panza, G. F., & Calcagnile, G. (1980). The gross features of the lithosphere-asthenosphere system in Europe from seismic surface waves and body waves. *Pure and Applied Geophysics*, *118*(2), 1209-1213.

Papazachos, B. C., & Comninakis, P. E. (1971). Geophysical and tectonic features of the Aegean arc. *Journal of Geophysical Research*, *76*(35), 8517-8533.

Papazachos, C., & Nolet, G. (1997). P and S deep velocity structure of the Hellenic area obtained by robust nonlinear inversion of travel times. *JOURNAL OF GEOPHYSICAL RESEARCH-ALL SERIES-*, *102*, 8349-8367.

Papazachos, B. C., Karakostas, V. G., Papazachos, C. B., & Scordilis, E. M. (2000). The geometry of the Wadati–Benioff zone and lithospheric kinematics in the Hellenic arc. *Tectonophysics*, *319*(4), 275-300.

Papoulia, J., & Makris, J. (2010). Tectonic processes and crustal evolution on/offshore western Peloponnese derived from active and passive seismics. *Bull. Geol. Soc. Greece*, *43*(1), 357-366.

Parker, R. L. (1972). The rapid calculation of potential anomalies. *Geophys. JR Astron. Soc*, *31*(4), 447-455.

Pasyanos, M. E. (2005). A variable resolution surface wave dispersion study of Eurasia, North Africa, and surrounding regions. *Journal of Geophysical Research: Solid Earth (1978–2012)*, *110*(B12).

Paton, s. (1992). Active normal faulting, drainage patterns and sedimentation in southwestern Turkey. *Journal of the Geological Society*, *149*(6), 1031-1044.

Pavlis, N. K., Holmes, S. A., Kenyon, S. C., & Factor, J. K. (2012). The development and evaluation of the Earth Gravitational Model 2008 (EGM2008). *Journal of Geophysical Research: Solid Earth (1978–2012)*, *117*(B4).

Pearce, F. D., Rondenay, S., Sachpazi, M., Charalampakis, M., & Royden, L. H. (2012). Seismic investigation of the transition from continental to oceanic subduction along the western Hellenic Subduction Zone. *Journal of Geophysical Research: Solid Earth (1978–2012)*, *117*(B7).

Pınar, A., & Kalafat, D. (1999). Source processes and seismotectonic implications of the 1995 and 1996 Cyprus, Eastern Mediterranean region, earthquakes. *Tectonophysics*, *301*(3), 217-230.

Piromallo, C., & Morelli, A. (1997). Imaging the Mediterranean upper mantle by P-wave travel time tomography.

Piromallo, C., & Morelli, A. (2003). P wave tomography of the mantle under the Alpine-Mediterranean area. *Journal of Geophysical Research: Solid Earth (1978–2012)*, *108*(B2).

Prelević, D., Akal, C., Foley, S. F., Romer, R. L., Stracke, A., & Van Den Bogaard, P. (2012). Ultrapotassic mafic rocks as geochemical proxies for post-collisional dynamics of orogenic lithospheric mantle: the case of southwestern Anatolia, Turkey. *Journal of Petrology*, *53*(5), 1019-1055.

Reilinger, R. E., McClusky, S. C., Oral, M. B., King, R. W., Toksoz, M. N., Barka, A. A. & Sanli, I. (1997). Global Positioning System measurements of present-day crustal movements in the Arabia-Africa-Eurasia plate collision zone. *Journal of Geophysical Research: Solid Earth (1978–2012)*, *102*(B5), 9983-9999.

Reilinger, R., McClusky, S., Vernant, P., Lawrence, S., Ergintav, S., Cakmak, R.& Karam, G. (2006). GPS constraints on continental deformation in the Africa-Arabia-Eurasia continental collision zone and implications for the dynamics of plate interactions. *Journal of Geophysical Research: Solid Earth (1978–2012)*, *111*(B5).

Richardson-Bunbury, J. M. (1996). The Kula volcanic field, western Turkey: the development of a Holocene alkali basalt province and the adjacent normal-faulting graben. *Geological Magazine*, *133*(03), 275-283.

Rimmelé, G., Jolivet, L., Oberhänsli, R., & Goffé, B. (2003). Deformation history of the high-pressure Lycian Nappes and implications for tectonic evolution of SW Turkey. *Tectonics*, *22*(2).

Ring, U., Johnson, C., Hetzel, R., & Gessner, K. (2003). Tectonic denudation of a Late Cretaceous–Tertiary collisional belt: regionally symmetric cooling patterns and their relation to extensional faults in the Anatolide belt of western Turkey. *Geological Magazine*, *140*(04), 421-441.

Ritzwoller, M. H., & Levshin, A. L. (1998). Eurasian surface wave tomography: Group velocities. *Journal of Geophysical Research: Solid Earth (1978–2012)*, *103*(B3), 4839-4878.

Rockwell, T., Barka, A., Dawson, T., Akyuz, S., & Thorup, K. (2001). Paleoseismology of the Gazikoy-Saros segment of the North Anatolia fault, northwestern Turkey: Comparison of the historical and paleoseismic records, implications of regional seismic hazard, and models of earthquake recurrence.*Journal of Seismology*, *5*(3), 433-448.

Romanowicz, B. A. (1980). A study of large-scale lateral variations of P velocity in the upper mantle beneath western Europe. *Geophysical Journal International*, *63*(1), 217-232.

Salah, M. K., Şahin, Ş., & Topatan, U. (2014). Crustal velocity and Vp/Vs structures beneath central Anatolia from local seismic tomography. *Arabian Journal of Geosciences*, *7*(10), 4101-4118.

Salaün, G., Pedersen, H. A., Paul, A., Farra, V., Karabulut, H., Hatzfeld, D.& Pequegnat, C. (2012). High-resolution surface wave tomography beneath the Aegean-Anatolia region: constraints on upper-mantle structure. *Geophysical Journal International*, *190*(1), 406-420.

Sari, C., & Şalk, M. (2006). Sediment thicknesses of the western Anatolia graben structures determined by 2D and 3D analysis using gravity data. *Journal of Asian Earth Sciences*, *26*(1), 39-48.

Saunders, P., Priestley, K., & Taymaz, T. (1998). Variations in the crustal structure beneath western Turkey. *Geophysical Journal International*, *134*(2), 373-389.

Savaşçın, M. Y., & Oyman, T. (1998). Tectono-magmatic evolution of alkaline volcanics at the Kırka-Afyon-Isparta structural trend, SW Turkey. *Turkish Journal of Earth Sciences*, *7*(3), 201-214.

Sayil, N., & Osmanşahin, İ. (2008). An investigation of seismicity for western Anatolia. *Natural Hazards*, *44*(1), 51-64.

Sayil, N. (2014). Determination of the Crust and Upper-Mantle Structure in Anatolia by Surface Wave Data. *Natural Science*, *6*(12), 968.

Schattner, U. (2010). What triggered the early-to-mid Pleistocene tectonic transition across the entire eastern Mediterranean? *Earth and Planetary Science Letters*, *289*(3), 539-548.

Schildgen, T. F., Cosentino, D., Caruso, A., Buchwaldt, R., Yıldırım, C., Bowring, S. A., Rojay, B., Echtler, H., & Strecker, M. R. (2012b). Surface expression of eastern Mediterranean slab dynamics: Neogene topographic and structural evolution of the southwest margin of the Central Anatolian Plateau, Turkey. *Tectonics*, *31*(2).

Schildgen, T. F., Yıldırım, C., Cosentino, D., & Strecker, M. R. (2014). Linking slab break-off, Hellenic trench retreat, and uplift of the Central and Eastern Anatolian plateaus. *Earth-Science Reviews*, *128*, 147-168.

Schmid, C., Van Der Lee, S., & Giardini, D. (2004). Delay times and shear wave splitting in the Mediterranean region. *Geophysical Journal International*, *159*(1), 275-290.

Şengör, A. M. C., (1979). The North Anatolian transform fault: its age, offset and tectonic significance. *Journal of the Geological Society*, *136*(3), 269-282.

Şengör, A. M. C., & Kidd, W. S. F. (1979). Post-collisional tectonics of the Turkish-Iranian plateau and a comparison with Tibet. *Tectonophysics*, *55*(3), 361-376.

Şengör, A. M.C., & Yilmaz, Y. (1981). Tethyan evolution of Turkey: a plate tectonic approach. *Tectonophysics*, *75*(3), 181-241.

Şengör, A. M.C., & Canitez, N. (1982). The North Anatolian Fault. *Alpine-Mediterranean Geodynamics*, 205-216.

Şengör, A. M. C., Görür, N., & Saroglu, F. (1985). Strike-slip deformation, basin formation and sedimentation: strike-slip faulting and related basin formation in zones of tectonic escape: Turkey as a case study. *Society of economic paleontologists and mineralogist, special publication*, *37*, 227-264.

Şengör, A. M. C., Özeren, S., Genç, T., & Zor, E. (2003). East Anatolian high plateau as a mantle-supported, north-south shortened domal structure. *Geophysical Research Letters*, *30*(24).

Seyitoglu, G., & Scott, B. C. (1992). The age of the Büyük Menderes graben (west Turkey) and its tectonic implications. *Geological Magazine*, *129*(02), 239-242.

Snopek, K., Meier, T., Endrun, B., Bohnhoff, M., & Casten, U. (2007). Comparison of gravimetric and seismic constraints on the structure of the Aegean lithosphere in the forearc of the Hellenic subduction zone in the area of Crete. *Journal of Geodynamics*, *44*(3), 173-185.

Sobolev, S. V., & Babeiko, A. Y. (1994). Calculation of phase equilibria and elastic properties of magmatic rocks. *Physics of the Solid Earth*, *30*, 931-947.

Sodoudi, F., Kind, R., Hatzfeld, D., Priestley, K., Hanka, W., Wylegalla, K.,& Bohnhoff, M. (2006). Lithospheric structure of the Aegean obtained from P and S receiver functions. *Journal of Geophysical Research: Solid Earth (1978–2012)*, *111*(B12).

Sodoudi, F., Brüstle, A., Meier, T., Kind, R., & Friederich, W. (2015). Receiver function images of the Hellenic subduction zone and comparison to microseismicity.

Spakman, W., & Nolet, G. (1988). Mathematical Geophysics: A Survey of Recent Developments in Seismology and Geodynamics.

Spakman, W. (1991). Delay-time tomography of the upper mantle below Europe, the Mediterranean, and Asia Minor. *Geophysical journal international*, *107*(2), 309-332.

Spakman, W., van der Lee, S., & van der Hilst, R. (1993). Travel-time tomography of the European-Mediterranean mantle down to 1400 km. *Physics of the Earth and Planetary Interiors*, *79*(1), 3-74.

Suckale, J., Rondenay, S., Sachpazi, M., Charalampakis, M., Hosa, A., & Royden, L. H. (2009). High-resolution seismic imaging of the western Hellenic subduction zone using teleseismic scattered waves. *Geophysical Journal International*, *178*(2), 775-791.

Talwani, M., Worzel, J. L., & Landisman, M. (1959). Rapid gravity computations for two-dimensional bodies with application to the Mendocino submarine fracture zone. *Journal of Geophysical Research*, *64*(1), 49-59.

Talwani, M., & Heirtzler, J. R. (1964). Computation of magnetic anomalies caused by two dimensional structures of arbitrary shape.

Taymaz, T., Jackson, J., & Westaway, R. (1990). Earthquake mechanisms in the Hellenic Trench near Crete. *Geophysical Journal International*, *102*(3), 695-731.

Taymaz, T., Westaway, R., & Reilinger, R. (2004). Active faulting and crustal deformation in the Eastern Mediterranean region. *Tectonophysics*, *391*(1), 1-9.

Telford, W. M., Geldart, L. P., & Sheriff, R. E. (1990). *Applied geophysics* (Vol. 1). Cambridge university press.

Tezcan, A. K. (1979). Geothermal studies, their present status and contribution to heat flow contouring in Turkey. In *Terrestrial heat flow in Europe* (pp. 283-292). Springer Berlin Heidelberg.

Tezcan, A. K., & Turgay, I. (1989). Heat Flow Map of Turkey, General Directorate of Mineral Research and Exploration (MTA), Department of Geophysics Research, Ankara (unpubl.).

Tezel, T., Erduran, M., & Alptekin, Ö. (2007). Crustal shear wave velocity structure of Turkey by surface wave dispersion analysis. *Annals of Geophysics*.

Tezel, T., Shibutani, T., & Kaypak, B. (2010). Crustal structure variation in western Turkey inferred from the receiver function analysis. *Tectonophysics*, *492*(1), 240-252.

Tezel, T., Shibutani, T., & Kaypak, B. (2013). Crustal thickness of Turkey determined by receiver function. *Journal of Asian Earth Sciences*, *75*, 36-45.

Tiberi, C., Diament, M., Caen, H. L., & King, T. (2001). Moho topography beneath the Corinth Rift area (Greece) from inversion of gravity data. *Geophysical Journal International*, *145*(3), 797-808.

Tirel, C., Gueydan, F., Tiberi, C., & Brun, J. P. (2004). Aegean crustal thickness inferred from gravity inversion. Geodynamical implications. *Earth and Planetary Science Letters*, *228*(3), 267-280.

Tokçaer, M.., Agostini, S., & Savaşçın, M. Y. (2005). Geotectonic setting and origin of the youngest Kula volcanics (western Anatolia), with a new emplacement model. *Turkish Journal of Earth Sciences*, *14*(2), 145-166.

Tonarini, S., Agostini, S., Innocenti, F., & Manetti, P. (2005). δ11B as tracer of slab dehydration and mantle evolution in western Anatolia Cenozoic magmatism. *Terra Nova*, *17*(3), 259-264.

Topuz, G., Altherr, R., Schwarz, W. H., Dokuz, A., & Meyer, H. P. (2007). Variscan amphibolite-facies rocks from the Kurtoğlu metamorphic complex (Gümüşhane area, Eastern Pontides, Turkey). *International Journal of Earth Sciences*, *96*(5), 861-873.

Tsokas, G. N., & Hansen, R. O. (1997). Study of the crustal thickness and the subducting lithosphere in Greece from gravity data. *Journal of Geophysical Research: Solid Earth (1978–2012)*, *102*(B9), 20585-20597.

Ustaömer, P., Mundil, R., & Renne, P. R. (2005). U/Pb and Pb/Pb zircon ages for arc-related intrusions of the Bolu Massif (W Pontides, NW Turkey): evidence for Late Precambrian (Cadomian) age. *Terra Nova*, *17*(3), 215-223.

Van Der Meijde, M., Van Der Lee, S., & Giardini, D. (2003). Crustal structure beneath broad-band seismic stations in the Mediterranean region. *Geophysical Journal International*, *152*(3), 729-739.

Van Hinsbergen, D. J. J., Hafkenscheid, E., Spakman, W., Meulenkamp, J. E., & Wortel, R. (2005). Nappe stacking resulting from subduction of oceanic and continental lithosphere below Greece. *Geology*, *33*(4), 325-328.

Van Hinsbergen, D. J. (2010). A key extensional metamorphic complex reviewed and restored: the Menderes Massif of western Turkey. *Earth-Science Reviews*, *102*(1), 60-76.

Vanacore, E. A., Taymaz, T., & Saygin, E. (2013). Moho structure of the Anatolian Plate from receiver function analysis. *Geophysical Journal International*, *193*(1), 329-337.

Villasenor, A., Ritzwoller, M. H., Levshin, A. L., Barmin, M. P., Engdahl, E. R., Spakman, W., & Trampert, J. (2001). Shear velocity structure of central Eurasia from inversion of surface wave velocities. *Physics of the Earth and Planetary Interiors*, *123*(2), 169-184.

Wdowinski, S., Ben-Avraham, Z., Arvidsson, R., & Ekström, G. (2006). Seismotectonics of the Cyprian arc. *Geophysical Journal International*, *164*(1), 176-181.

Westaway, R. (2006). Cenozoic cooling histories in the Menderes Massif, western Turkey, may be caused by erosion and flat subduction, not low-angle normal faulting. *Tectonophysics*, *412*(1), 1-25.

Whitney, D. L., & Hamilton, M. A. (2004). Timing of high-grade metamorphism in central Turkey and the assembly of Anatolia. *Journal of the Geological Society*, *161*(5), 823-828.

Wortel, M. J. R., & Spakman, W. (2000). Subduction and slab detachment in the Mediterranean-Carpathian region. *Science*, *290*(5498), 1910-1917.

Yiğitbaş, E., Kerrich, R., Yılmaz, Y., Elmas, A., & Xie, Q. (2004). Characteristics and geochemistry of Precambrian ophiolites and related volcanics from the Istanbul–Zonguldak Unit, Northwestern Anatolia, Turkey: following the missing chain of the Precambrian South European suture zone to the east. *Precambrian Research*, *132*(1), 179-206.

Yilmaz, Y., Genç, Ş. C., Gürer, F., Bozcu, M., Yilmaz, K., Karacik, Z.,& Elmas, A. (2000). When did the western Anatolian grabens begin to develop?. *Geological Society, London, Special Publications*, *173*(1), 353-384.

Yolsal-Cevikbilen, S., Biryol, C. B., Beck, S., Zandt, G., Taymaz, T., Adiyaman, H. E., & Özacar, A. A. (2012). 3-D crustal structure along the North Anatolian Fault Zone in north-central Anatolia revealed by local earthquake tomography. *Geophysical Journal International*, *188*(3), 819-849.

Zhu, L., Mitchell, B. J., Akyol, N., Cemen, I., & Kekovali, K. (2006). Crustal thickness variations in the Aegean region and implications for the extension of continental crust. *Journal of Geophysical Research: Solid Earth (1978–2012)*, *111*(B1).

Zonenshain, L. P. (1975). Problems of global tectonics. *AAPG Bulletin*, *59*(1), 124-133.

Zor, E., Sandvol, E., Gürbüz, C., Türkelli, N., Seber, D., & Barazangi, M. (2003). The crustal structure of the East Anatolian plateau (Turkey) from receiver functions. *Geophysical Research Letters*, *30*(24).

Zor, E., Özalaybey, S., & Gürbüz, C. (2006). The crustal structure of the eastern Marmara region, Turkey by teleseismic receiver functions. *Geophysical Journal International*, *167*(1), 213-222.